Nearshore bathymetric changes along the Alaska Beaufort Sea coast and possible physical drivers

by

Mark Zimmermann[1], Li H. Erikson[2], Ann E. Gibbs[2], Megan M. Prescott[3†], Stephen M. Escarzaga[4], Craig E. Tweedie[4], Jeremy L. Kasper[5], and Paul X. Duvoy[5]

[1]contact author Email: mark.zimmermann@noaa.gov, Voice (206) 526-4119.

National Marine Fisheries Service, NOAA, Alaska Fisheries Science Center, 7600 Sand Point Way NE, Bldg. 4, Seattle, WA, 98115-6349, USA.

[2]U.S. Geological Survey, Pacific Coastal and Marine Science Center, 2885 Mission Street Santa Cruz, CA 95050, USA; lerikson@usgs.gov and agibbs@usgs.gov.

[3]Lynker Technologies, Under contract to Alaska Fisheries Science Center, 7600 Sand Point Way NE, Bldg. 4, Seattle, WA 98115-6349, USA; megan.prescott@noaa.gov.

[4]Department of Biological Sciences, University of Texas El Paso, 500 W University Ave, El Paso, TX 79968, USA; smescarzaga@utep.edu and ctweedie@utep.edu.

[5]Alaska Center for Energy and Power, University of Alaska Fairbanks, PO Box 755910, Fairbanks, AK 99775-5910, USA; jlkasper@alaska.edu and pxduvoy@alaska.edu.

[†] Present address: Dewberry, 990 S Broadway #400, Denver, CO 80209

Abstract

Erosion rates along Alaska's Beaufort Sea coast, among the highest in the world, are negatively impacting communities, industrial and military infrastructure, and wildlife habitat. Decreasing maximal winter ice extent and increasing summer open water duration and extent in the Beaufort Sea may be making the coast more vulnerable to destructive storm waves than during recent, colder, icier decades. Previous studies of Beaufort Sea coastal change have been limited to subaerial analyses of the shoreline. Here we describe nearshore seafloor change by comparing post-World War II (WWII) (1945-53) bathymetry data to recently acquired (1985-2018) bathymetry data and relate the observed seafloor change to adjacent shoreline change near Utqiagvik, within Stefansson Sound, and immediately west of Barter Island and Kaktovik. Within the Utqiagvik region, seabed erosion was generally highest (> 1.0 m of loss) offshore of Point Barrow and along the eastern end of the Tapkaluk Islands, while there were lesser amounts of deposition (< 0.5 m of gain) within the protected waters of Elson Lagoon. Sedimentation was generally highest offshore of Point Barrow, in a region of converging currents, and on the landward side of the barrier islands and spits fronting Elson Lagoon, which is likely related to a regional trend of westerly sediment transport and landward migration of the barrier islands. Within Stefansson Sound, perhaps the most notable changes from post-WWII bathymetry data compared to recent data are a switch from mixed, low erosion and deposition in 1997 to low deposition (< 0.5 m) in 2018 east of the Boulder Patch, a switch from low erosion in 1997 to neutral depth change in 2018 in the channel between the north and south Boulder Patch areas, and higher deposition from 1997 to 2018 landward of the rapidly retreating barrier islands along the Sound’s northern border. At Barter Island, high erosion near north-facing shorelines and high deposition near west-facing shorelines generally matched shoreline changes. One of our goals is

to identify possible processes responsible for the depth changes we quantified. Using simple metrics that relate sediment characteristics with modeled waves and non-wave induced currents, we show that sediment resuspension and transport by both wave and non-wave driven currents likely contribute to the overall patterns of change within the ~13 m isobath along the open coast , and that the influence of wave action affecting sediment transport is expanding seaward.

1. Introduction

The Beaufort Sea coast of Alaska is experiencing rapid change as Arctic summer sea ice is receding faster than previously projected (Overland et al., 2019; Kumar et al., 2020; Richter-Menge and Druckenmiller, 2020), and air and ocean temperatures, permafrost thaw, and ocean wave energy are increasing (Overeem et al., 2011; Thomson et al., 2016; Biskaborn et al., 2019; Timmermans and Ladd, 2019; Lim et al., 2020; Nederhoff et al., 2021). These changes lead to increased vessel traffic, opportunities for coastal and offshore development, and increased vulnerability of communities and built coastal environments to erosion. Impacts to marine ecosystems (e.g., Logerwell et al., 2015) are also highly likely but climate change aspects are only just beginning to be incorporated in biological studies (e.g., Laurel et al., 2017; Vestfals et al., 2021). Based on a spatially comprehensive shoreline change analysis extending from the Canadian border to Point Barrow (Figure 1A), some of the highest shoreline change rates in the world, over 20 m/yr, have been measured at distinct locations on Alaska's Beaufort Sea coast (e.g., Mars and Houseknecht, 2007; Gibbs and Richmond, 2015; 2017) a phenomena first reported over a century ago (Leffingwell, 1908). A corresponding change analysis of the nearshore subaqueous environment, which is critical for habitat assessments (e.g., fisheries surveys) and understanding physical processes associated with erosion and flooding, has not yet been done. Such an analysis would be limited due to the sparse geographic coverage and low

quality of available nearshore bathymetry data, but with well-tested methods of correcting older hydrographic data sets (Zimmermann and Benson, 2013), it is now possible, within small regions, to ascertain nearshore bathymetric changes compared to historic soundings in Alaska dating back to the post-World War II (WWII) (1945-53) era. The goal of this work is to quantify inner shelf bathymetric change at locations where recent (since 1985) and historic overlapping data exist (Utqiagvik region Figure 1B; Stefansson Sound region Figure 1C; and Barter Island region Figure 1D), and to identify possible processes responsible for the changes. Analysis of bathymetric change, in combination with documented shoreline change rates, waves, currents, sediment types (Buczkowski et al., 2020a; 2020b), fluvial sediment loads, and sea ice can provide a first order assessment of source inputs and physical drivers such as critical shear stress and the depth-of-closure or DOC that contribute to sediment transport pathways and redistribution patterns. This information can be an important component in evaluating morphological and physical processes associated with coastal change and understanding future vulnerabilities. As additional nearshore bathymetric, sedimentological, and process datasets are acquired, this methodology can be expanded to improve the understanding of the linkage between offshore and onshore processes and sediment transport pathways.

1.1 Study area and history

The Beaufort Sea coast of Alaska extends about 630 km in length from Point Barrow, on the edge of the Chukchi Sea in the west, to the U.S.-Canadian border near Demarcation Bay in the east (Figure 1A). Numerous bays incise the coast and numerous barrier islands parallel the coast at a distance of about 1 to 17 km from the mainland shore, providing some protection from wave-driven coastal change processes. Several major rivers drain the coastal plain between the

Beaufort Sea coast and the Brooks Range, delivering freshwater and sediment to the bays through large river deltas (Figure 1A).

Although sea ice offers coastal protection from storm waves for about nine months of the year, the Beaufort seabed is also commonly gouged by sea ice, with some areas of the shelf completely covered by ice gouges (Barnes et al., 1984; Barnes and Rearic, 1985; Wolf et al., 1985; Rearic, 1986; Rearic and Ticken, 1988; Horowitz, 2002), requiring many years for full benthos recolonization (Conlan and Kvitek, 2005). Ice gouges are more prevalent offshore of barrier islands where ice-mass pressure ridges develop deep keels capable of dredging > 5 m deep incisions into the seabed (Reimnitz and Barnes, 1974). Within protected areas between barrier islands and the mainland coast, ice gouges are significantly shallower (< 0.5 m) and less prevalent (Reimnitz and Barnes, 1974; Coastal Frontiers, 1997 cited in Hearon et al., 2009). Ice gouges are most frequent between the 15 and 25 m isobaths in the "stamukhi zone" where the landfast ice terminates and the mobile pack ice impinges on the immobile landfast ice, creating deep pressure ridges that help to anchor the landfast ice in place (Barnes et al., 1984; Mahoney et al., 2007).

During spring/early summer ice break-up, coastal rivers discharge warmer, fresh, sediment-laden water at the coast, hastening nearshore melting. Freshwater from rivers flows both underneath the sea ice (Alkire and Trefry, 2006) and penetrates the ice cover from above through stress or thermal cracks and seal breathing holes, forming "strudel" vortices which can scour bottom sediments. This process also freshens the surface waters and disperses large amounts of sediment and organic matter into the water column (Reimnitz and Kempema, 1983).

Coastal Frontiers Corporation identified and measured numerous strudel scours, <1 m in depth and mostly circular in shape, within Foggy Island Bay (FIB) in Stefansson Sound (Hearon

et al., 2009). Linear scours, ranging up to 2.4 m deep and 39.6 m long, and formed by drainage through elongated "tidal" cracks at the offshore limit of the bottom fast ice, were observed but less common. Using measurements within FIB and other regions of the North Slope, Hearon et al. (2009) concluded that strudel scouring is most widespread and frequent within the seaward edge of the bottom fast ice edge (~1.5 m isobath) out to the 6 m isobath.

The Beaufort Sea coast and nearshore seafloor has been comprehensively mapped only once, by the U.S. Coast and Geodetic Survey, a precursor agency of the NOS (National Ocean Service), just after WWII (1945 to 1953). Initially, topographic or T-sheets were prepared, showing the shoreline and positions of newly established triangulation stations. Afterwards, the hydrographic or H-sheets, also known as smooth sheets, were prepared by conducting bathymetric surveys that utilized the T-sheet shorelines and triangulation stations for navigation. The H-sheets are more detailed (typically 1:20,000) records of hydrographic surveys than the relatively low-resolution NOS navigational charts that were derived from them (Zimmermann and Benson, 2013).

T-sheet shorelines and H-sheet bathymetry data are used frequently for both navigation and change detection studies (for example, Gibbs and Richmond, 2015; Gibbs et al., 2019b; Zimmermann et al., 2018; Zimmermann et al., 2019a), and smooth sheet data are also used for modeling fish and invertebrate habitats (Rooper et al., 2014; Rooper et al., 2016; Zimmermann et al., 2016; Laman et al., 2017; Turner et al., 2017; Rooney et al., 2018; Baker et al., 2019), hydrographic modeling (Martin et al., 2015; Wang and Yang, 2020), and geomorphological analyses (Zimmermann and Prescott, 2018; Zimmermann et al., 2019b; Jakobsson et al., 2020; Zimmermann and Prescott, 2021a; 2021b). Unfortunately, some of the historical data archived digitally at NOAA's (National Oceanic and Atmospheric Administration) National Centers for

Environmental Information portal (NCEI, http://www.ngdc.noaa.gov/) have been found to be incomplete, incorrect, and/or not accurately georeferenced (Zimmermann and Benson, 2013).

Researchers at NOAA's Alaska Fisheries Science Center (AFSC) identified numerous errors in the digital smooth sheet sounding data at locations throughout Alaska and developed a methodology of recreating the georegistration process so that the digitized sounding data from NCEI could be corrected (Zimmermann and Benson, 2013). These corrections were applied to the smooth sheet data used in this study along the Alaskan Beaufort Sea coast and are discussed further in the data and methods section.

Researchers at the United States Geological Survey (USGS) used the post-WWII T-sheets, along with aerial and satellite imagery, and LiDAR (Light Detection and Ranging) elevation data from 4 time periods (circa 1940s, 1980s, 2000s, and 2010s) to calculate shoreline change rates along the Alaska Beaufort Sea coast every 50 m alongshore over two time periods: long-term (LT; 1940s to 2010s), and short-term (ST; 1980s-2010s) (Gibbs and Richmond, 2015; 2017). Shoreline change rates were not calculated near river deltas. Results show that the coast was dominantly erosional over the LT with 88 percent of transects exhibiting shoreline retreat. Mean LT shoreline change rates of -1.8 ± 0.1 m/yr over the entire study area were not significantly different than the ST -1.9 ± 0.1 m/yr. Rates were highly variable, however, ranging from -25 to +20 m/yr, with extreme rates associated with migration of barrier islands and limited sections of the mainland coast. Shorelines were generally more erosional during the ST compared to the LT, particularly west of the Colville River. Increases in mean erosion and accretion, along with an increase in the percent of the coast accreting, indicate that the coast is changing more rapidly through time. This is particularly important on the exposed mainland coast where loss of the permafrost bluff and tundra landscape is permanent, and the eroded

material is entrained into the littoral system, redistributed, and deposited as more ephemeral and dynamic beach, spit, mud flat, and barrier island landforms.

2. Data and methods

The NOS created 40 hydrographic smooth sheets of the Beaufort Sea between 1945 and 1953 (Table 1), providing a record of about 0.25 million fathometer (early singlebeam) soundings within a very narrow (~< 20 km), shallow (~< 20 m) band along the coast (Figure 1A). Notes on the smooth sheets and comments in the associated Descriptive Reports indicate that offshore survey efforts were limited in places by the presence of the permanent Arctic ice pack (e.g., H07760) and, in some cases, by grounded ice floes, features described as “icebergs” by the hydrographers (e.g., H07856, H07857). Extensive nearshore areas, occurring between the shallowest soundings and the shoreline, were too shallow for safe navigation of the hydrographic survey vessels and not surveyed. These unmapped, nearshore areas were often left blank on charts and consequently referred to as "white zones" or “holidays” by cartographers.

2.1 Historical hydrographic data

Most of the materials for this project come from the NCEI, which hosts hydrographic data and imagery from the NOS. Zimmermann and Benson (2013) describe the detailed methods for proofing, editing, digitizing, and plotting historical smooth sheet soundings from NCEI, and here we report these methods in brief for the 40 smooth sheet surveys used in this project; 38 of which were digitized for NCEI, and two (F00109 and H07761) with no digital soundings data available from NCEI. Through a georegistration and digitization process, digital data files of the smooth sheet soundings were created and archived at NCEI, but unfortunately without any proofing (Wong et al., 2007) and without details on exact methodologies. These digitized hydrographic soundings, digital images of the smooth sheets, and scans of the associated

Descriptive Reports were downloaded from NCEI. Smooth sheet images were georegistered to a common horizontal datum (the North American Datum of 1983 or NAD83) in ArcMap (v.10.2.2, ESRI: Environmental Systems Research Institute, Redlands, CA), using locations of common triangulation stations from NOAA, National Geodetic Survey (http://www.ngs.noaa.gov/cgi-bin/sf_archive.prl). The digitized sounding data accessed from NCEI were compared to sounding locations plotted on the smooth sheets (the hand-inked numerals representing sounding depths) that we correctly georegistered. We determined that all 38 of the smooth sheets had been incorrectly georegistered prior to the digitizing of the locations of the bathymetric soundings done for NCEI, likely due to misunderstandings about the smooth sheet horizontal datums (Zimmermann and Benson, 2013). To correct this, all soundings on a smooth sheet were shifted horizontally (from a minimum of 100 m to a maximum of 9300 m) using ArcMap's Editor to align with the correctly georegistered smooth sheets (Table 1). By comparing the 38 digital files of soundings from NCEI to the 38 properly georegistered smooth sheets, missing soundings were digitized, erroneously digitized soundings were corrected, and duplicate soundings were deleted. Soundings from the remaining two smooth sheets (F00109 and H07761) were digitized as part of this study.

Hydrographers collected the depth soundings in units of 1 ft (0.305 m) and corrected them to a vertical datum of Mean Lower Low Water (MLLW) by utilizing temporary tide stations installed at each survey site for the duration (~weeks) of each hydrographic survey, since a permanent tide station was not available. Mean High Water (MHW), defined as the shoreline, was determined to be less than 1 ft (0.305 m) above MLLW for each smooth sheet survey using the same tide measurements. Because of the low tidal range in the region (21 cm [0.7 ft] diurnal range at the permanently recording tide station at Prudhoe Bay [NOAA, 2021]), potential tidal

measurement errors were not considered to be a significant factor in the hydrographic measurements.

The post-WWII bathymetric soundings provide the only moderately complete set of depth measurements in this area. To facilitate a better understanding of depth change over time, we created a TIN (Triangulated Irregular Network) from these early, correctly georeferenced depth soundings, converted the TIN into a 100-m horizontal resolution raster surface, and utilized this raster for creating 2-m interval depth contours and also for comparing the interpolated raster cell values to the recent bathymetric sounding data (points) – all in ArcMap.

2.2 Recent hydrographic data

The nearshore Alaska Beaufort Sea coast has not been comprehensively resurveyed since this initial post-WWII mapping effort, however, there have been limited regional and localized bathymetric survey efforts including two shallow water multibeam surveys and several singlebeam surveys that partially overlap with the historical smooth sheets (Table 2; Figure 1). Hydrographers conducted a multibeam cruise on the *Fairweather* in 2015 (NCEI), producing a 32 m horizontal resolution grid (D00168) along the full length of the Alaskan Beaufort Sea coast, with zigzagging onshore/offshore transects and numerous closely spaced transects near Point Barrow (Figure 1A). Hydrographers also conducted a multibeam survey with two *Fairweather* launches in 2012 (NCEI), producing a 50 m horizontal resolution grid (F00666), in a small area off Elson Lagoon, for comparison to satellite-derived bathymetry (Figure 1A). Singlebeam bathymetry was collected in Elson Lagoon in 2015 (C. Tweedie, personal communication; Figure 1B), in Foggy Island Bay / Stefansson Sound in 1985, 1997 and 2018 (Hachmeister et al., 1985; Danek and Tourtellotte, 1987; Short et al., 1991; Coastal Frontiers, 2014; Kasper et al., 2019; Figure 1C), and near Barter Island in 2011 (Erikson et al., 2020; Figure 1D). Unfortunately

we found that some of the 1985 singlebeam soundings from Stefansson Sound, which we refer to as the Endicott 1985 data set, plotted on top of the permanent Endicott Causeway, rather than around it, as shown in Danek and Tourtellotte (see Figure 1: 1987), indicating a navigational problem with the data. This Causeway connects the Endicott Main Production Island and the Endicott Satellite Drilling Island, all constructed in the mid-1980s to facilitate petroleum production and delivery, to the mainland. We attempted to fix this navigational problem but ultimately decided that it was too complex for this project and therefore we did not utilize Endicott 1985 further in this project. Technically, the 2018 Stefansson Sound data were multibeam (Kasper et al., 2019) but for the large surveyed area, we determined that using the original multibeam survey provided a marginal advantage over using the same data converted to a narrow path of soundings, with a considerable reduction of data size. Elson Lagoon data were reported relative to NAD83 (2011) ellipsoidal elevations and converted to MLLW depths by shallowing depths by 2.099 m, using conversion information from the Alaska Tidal Datum Portal for the Barrow Offshore tide station (https://dggs.alaska.gov/hazards/coastal/ak-tidal-datum-portal.html). Stefansson Sound data were converted from MSL to MLLW by shallowing depths by 0.106 m as determined from the published offsets at Prudhoe Bay (https://tidesandcurrents.noaa.gov/datums.html?id=9497645). Arey/Barter Island bathymetry data were published relative to a MSL datum and converted to MLLW datum by shallowing depths by 0.085 m, as determined from the published offsets at Barter Island (https://tidesandcurrents.noaa.gov/datums.html?id=9499176).

2.3 Bathymetry comparison

ESRI ArcMap's "Extract Values to Points" tool in Spatial Analyst was used to compare point and raster data sets from different eras. In this method, a single point from one data set

falling inside of a raster cell from another data set constitutes a comparison, but raster cells may be compared to multiple points. Since the recent multibeam data sets (F00666 in 2012 and D00168 in 2015) were already available as rasters, we extracted those raster cell values to the NOS smooth sheet soundings as one means of comparison. The recent singlebeam data sets were not available as rasters, and generally not suitable for generating rasters due to linear, widely spaced transects, so we used the extraction method in the opposite direction, comparing cell values from the 100-m NOS smooth sheet raster to individual recent singlebeam points, for identifying possible depth change over time. We report summarized depth change comparisons with the sample size (n), mean ($\bar{x}$), and ± standard deviation (SD).

Even with our focus on using well-established methods to correct the older smooth sheet data, it was not known if potential digitization errors could be identified and corrected sufficiently enough in these Beaufort Sea data sets to provide meaningful overlaps with newer bathymetry data sets in this area of ongoing coastal change research. It was also not known if seafloor ice gouging, and strudel or linear scours, would result in a noisy depth change comparison, or if the data preparation methods would produce results showing clear, spatially coherent sediment erosion and deposition signals from wind- and wave-driven currents, similar to the strongly autocorrelated patterns of erosion and progradation in the shoreline (Gibbs and Richmond, 2015; 2017).

2.4 Currents as physical drivers

The potential for currents to entrain and transport seabed sediment was assessed by computing maximum bed shear stresses exerted by oceanic flows and comparing these to critical shear stresses necessary to initiate motion and transport sediment with characteristics derived

from the usSEABED database (Buczkowski et al., 2020a; 2020b). Site-specific bed shear stresses were estimated with,

$$\tau_o = \rho C_{100} U_{100}^2 \,, \quad (1)$$

where ρ is the water density (=1028 kg/m^3), $C_{100}$is the drag coefficient, here set at 0.0024 for mixed sand/gravel seabeds (Soulsby, 1983), and U_{100} is the current speed at ~1m above the seabed. In this study, U_{100} was taken as the maximum near-bed velocities obtained with the high-resolution regional ROMS circulation model of Beaufort Sea nearshore areas (Curchitser et al., 2017) for the 2015 ice-free season (July 01- September 14). The nearshore Beaufort Sea ROMS model is a 3-grid nested state-of-the-science coupled circulation and sea ice numerical ocean model used to simulate horizontal and vertical ocean currents and ice for the years 1999 through 2015. Results from the finest 0.5 km resolution grid were used to describe maximum bottom currents at Stefansson Sound and Barter Island. The finest grid did not encompass the Utqiagvik study area and thus results from a 3-km resolution grid were used for analyses surrounding Point Barrow and within Elson Lagoon.

The critical shear stress, or threshold of motion under the influence of currents, was calculated with the empirical formula (Soulsby and Whitehouse, 1997; Soulsby, 1997),

$$\theta_{cr} = \frac{0.30}{1+1.2D_*} + 0.055[1 - exp(-0.020D_*)] \quad (2)$$

and $D_* = \left[\frac{g(\rho s/\rho - 1)}{\gamma^2}\right]^{1/3} d_{50}$,

where ρs is the grain density (2650 kg/m^3), g is the acceleration of gravity (9.83 m/s^2 at N72°), γ is the kinematic viscosity of water, and d_{50} the median grain size diameter. γ is dependent on water salinity and temperature, here taken to range from 25 to 35psu and 2 to 10°C, respectively.

2.5 Waves as physical drivers

The potential for waves being a cause for the observed nearshore sediment-erosion patterns was evaluated by estimating the depth at which the historical wave climate was sufficiently energetic to move seabed sediment. The depth-of-closure for a given or characteristic time interval is the most landward depth seaward of which there is no significant change in bottom elevation and no significant net sediment transport between the nearshore and offshore region (Kraus et al., 1998).

Describing the threshold of seabed agitation by wave action, Hallermeier (1981; 1983) derived equations for the inner and outer closure depth;

$$h_{in} = 2.28H_{s12h/yr} - 68.5\left(\frac{H_{s12h/yr}^2}{gT^2}\right), \quad (3a)$$

$$h_{out} = 0.013H_sT_s\sqrt{g/(1.65d_{50})} \quad (3b)$$

where $H_{s12h/yr}$ is the effective wave height (m) just seaward of the breaker zone that is exceeded more than 12 hours per year (i.e., the significant wave height with a probability of yearly exceedance of 0.137%), T the wave period (s) associated with $H_{s12h/yr}$, and H_s and T_s the annual mean significant wave height and mean period.The variable h_{in} marks the transition from the upper to lower shoreface where nearshore waves and wave induced currents are the dominant sediment-transport mechanisms. The variable h_{out} marks the transition where the influence of wave action on cross-shore sediment transport is likely to be insignificant.

Closure depths were calculated using the ERA5 wave reanalysis (C3S, 2017). ERA5 reanalysis wave products are generated globally on a 0.5° (~30 km at N70°) grid from a numerical wave model forced by altimeter-derived winds and further adjusted by assimilating altimeter-derived wave observations. ERA5 is comprised of hourly outputs across the entire globe from 1979 to present. Outputs from the closest grid points to Barrow (N71.5°, W156.5°),

Foggy Island Bay (N70.5°, W147.5°), and Barter Island (N70.5°, W144°), in ~20 m water depth, were used to estimate h_{out}, and additionally h_{in} after shoaling the wave time-series to a 10 m water depth (estimated to be outside the breaking zone) using linear wave theory. Annual h_{in} and h_{out} were calculated from 1979 through 2019 using Eq. (3a and 3b).

3. Results

Bathymetric change comparisons near Utqiagvik are concentrated north of Point Barrow, seaward of the Tapkaluk Islands, and within Elson Lagoon (Figure 2). Within Stefansson Sound, bathymetric change comparisons are concentrated near Foggy Island Bay, around the Boulder Patch and its rich and diverse kelp bed community (Dunton et al., 1982; Martin and Gallaway, 1994), and the offshore barrier islands (Figure 3A&B). Lastly, we assess overlapping singlebeam data with NOS soundings along the nearshore exposed coast of western Barter Island, Arey Island, and within Arey Lagoon (Figure 4).

Resolution of the older smooth sheet bathymetry data is rather coarse (0.305 m vertical resolution and with unknown horizontal resolution) and uncertainties are not quantified in the accompanying documentation. After considering uncertainties in modern hydrographic data, we assign low confidence in any depth changes smaller than 0.50 m or where the variability is greater than one SD. While some researchers have created observation error estimates for depth soundings using institutional performance measures, rather than from individual surveys or soundings (e.g., Buster and Morton, 2011; Latapy et al., 2019), we have avoided this due to uncertainty about what those errors might be.

There are always questions about the quality of these older smooth sheet bathymetry data sets and the appropriateness of their use for analyses, as many researchers simply download and plot the raw data from NCEI without any proofing and editing. Skipping these important data

processing steps results in chaotic and nonsensical seafloor maps (e.g., soundings plotting on land) that make it seem as if these older data are fundamentally flawed, and therefore unusable (Calder, 2006). Throughout this study we have taken great care in considering horizontal positioning errors and, for example, identified and addressed such errors in Stefansson Sound that subsequently allowed for depth change analyses that could not have been done with the uncorrected data (further described in Section 3.2).

3.1 Utqiagvik region

Bathymetric comparisons offshore of Point Barrow are generally close to shore (< 10 km), in shallow water (mostly < 12 m in depth) and occur in distinctive regions with relatively uniform amounts of erosion and deposition (Figure 2). There are three nearly continuous bands of consistent depth change parallel and seaward of the Barrow Spit shore from Point Barrow to Eluitkak Pass, alternating between erosion, deposition, and erosion. These bands may be alongshore bars (as observed by Short, 1973; 1975, for example); such bars are typically dynamic, migrating on a seasonal scale, and as such could represent only a snap-shot in time rather than a long-term change. However, closest to shore (< 600 m) of the moderate to rapidly eroding (up to 3 m/yr) spit east of Point Barrow is a discontinuous band of large seabed erosion (mostly < 3.4 m), demonstrating the linked behavior between nearshore and beach erosion and perhaps indicating that profile steepening or related processes are driving both seafloor and beach erosion in this area (Gibbs and Richmond, 2015; 2017) (n=14, mean or $\bar{x}$ = 1.51 m, ± 0.59 SD; Figure 2(a)). Offshore of that band of erosion, at a distance of about 800 to 1000 m from shore, is a discontinuous band of high deposition ranging up to almost 3 m of accumulated sediment (n=10, $\bar{x}$ =-1.81 m, ± 0.61; Figure 2(b)). At a distance of about 800 to 1,300 m offshore is a third discontinuous band of relatively consistent depth change, showing erosion of up to 3.2

m (n=9, $\bar{x}$ =1.65 m, ± 0.71; Figure 2(c)). The western tip of Point Barrow shows high rates of shoreline progradation, and about 2.5 km directly north of this area is a continuous seafloor region of relatively large deposition (< 2.3 m) occurring between 8 and 10 m water depth (n=52, $\bar{x}$ =-0.85 m, ± 0.46; Figure 2(d)). Only about 3 km to the east of this area of deposition is a mixed region with mostly moderate (< 2.5 m) erosion values (n=103, $\bar{x}$ =0.66 m, ± 0.39; Figure 2(e)), while about another 3 km to the east is an area mostly of lower values of deposition (< 0.7 m; n=42, $\bar{x}$ =-0.20 m, ± 0.20; Figure 2(f)).

There are fewer depth comparisons available offshore of the Tapkaluk Islands, but they are similarly close to shore (< 5 km) and shallow in depth (< 12 m) as at Point Barrow (Figure 2). At the eastern end of the Tapkaluk Islands, in an area of moderate to very high shoreline erosion (up to 11 m/yr), there is a group of bathymetric comparisons distributed in a narrow band paralleling the shore in shallow water (n=9, < 5 m depth), all showing high erosion values (1.2 to 2.2 m; n=9, $\bar{x}$ =1.71 m, ± 0.38; Figure 2(g)). Just offshore of this nearshore band of erosion is a group of bathymetric comparisons with moderate (< 1.0 m; Figure 2(h)) erosion in slightly deeper water (5-7 m depth; n=6, $\bar{x}$ =0.66 m, ± 0.07). Still farther offshore, between about 10-12 m water depth, is a group of mixed erosional and depositional bathymetric comparisons, but with most (25 of 29) observations showing erosion values of less than about 0.7 m ($\bar{x}$ =0. 26 m, ± 0.24; Figure 2(i)). Farther to the west along the Tapkaluk Islands, nearer to an area of minimal shore erosion and accretion, a group of 15 bathymetric comparisons shows consistent but low amounts of deposition (< 0.4 m; $\bar{x}$ = -0.18 m, ± 0.10; Figure 2(j)). The offshore area of low erosion (Figure 2(i)) and the western area of low deposition (Figure 2(j)) may potentially define the boundaries of this large area of high (Figure 2(g)) and moderate (Figure 2(h)) nearshore erosion.

Depth changes in Elson Lagoon are more moderate than in the offshore region, perhaps because the lagoon is relatively shallow (mostly < 4 m) and protected by islands and spits (Figure 2). The largest depth changes occur in areas adjacent to eroding barrier islands and spits around the perimeter of the lagoon and a scatterplot of all the data within the lagoon summarizes the predominantly (93,369 out of 136,583, or 68%) depositional pattern (Figures 2 and 5A). The highest deposition values (mostly > 1.0 m and ranging up to 9.0 m) occur mostly on the western and eastern sides of Eluitkak Pass, in the pass between Deadmans Island and the Tapkaluk Islands, near the southern half of Barrow Spit, and at the eastern entrance to the lagoon (n= 4,937, $\bar{x}$ = -1.44 m, ± 0.93; Figure 2(k)). Deposition values of < 1 m in the north and center of the lagoon, near inlets between the barrier islands (n= 3,594, $\bar{x}$ = -0.58 m, ± 0.14; Figure 2(l)), decrease to < 0.5 m in much of the western and eastern areas of the lagoon (n= 64,302, $\bar{x}$ = -0.21 m, ± 0.14; Figure 2(m)), illustrating a distinct trend of decreasing deposition farther away from the barrier island passes. This deposition within the lagoon, covering an area of about 125 km^2 with about 0.026 km^3 of sediment, is quite a noteworthy reduction of water volume since the lagoon was already shallow prior to the deposition. Less than a third of the lagoon comparison sites indicate erosion, and less than one percent indicate erosion > 1 m, with the highest erosion values (4.0 to 4.8 m) occurring within Eluitkak Pass (n=165, $\bar{x}$ = 2.66 m, ± 1.14; Figure 2(n)). Low amounts of erosion, almost all < 1 m, were measured in the southwestern, shallow corner of the lagoon, in Iko Bay, and near Point Ross at the eastern boundary of the lagoon (n= 3,065, $\bar{x}$ = 0.63, ± 0.14; Figure 2(o)).

3.2 Stefansson Sound

According to the Bathymetric Data Viewer at NCEI (https://www.ncei.noaa.gov/maps/bathymetry/) there are no post-WWII NOS smooth sheet

surveys covering Stefansson Sound, creating a large gap in survey coverage along the Beaufort Sea coast and potentially eliminating this important study site from our project. However, by shifting the soundings from H07760 about 9,300 m to the southwest to align with the correctly georegistered smooth sheet, and by completely digitizing the soundings from H07761 (Table 1), we determined that this area had been thoroughly surveyed (Figure 1A). Therefore we were able to make depth change comparisons to multiple recently collected bathymetry data sets.

Overall, the Coastal Frontiers 1997 data are weighted toward being more erosional than depositional (Figure 5B). An exception exists in the vicinity of the post-WWII 5m isobath where deposition dominates (as shown with the vertical scatter of data points against the vertical axis representing modern bathymetry). The UAF 2018 data show similar results but with greater erosion between the modern 6 m and 10 m isobath. Seaward of the modern day 10 m isobath, the slight erosion dominates and with little variance.

Looking closer at the spatial patterns, the Coastal Frontiers 1997 data generally show low amounts (< 0.5 m) of erosion within the Boulder Patch (as digitized from Bonsell and Dunton, 2018) since the post-WWII NOS data were collected, but higher variability around its edges. Low amounts (< 0.5 m) of both erosion and accretion were measured east of the Boulder Patch (n= 1,824, $\bar{x}$ = 0.07 m, ± 0.16; Figure 3A(a)) indicating a lack of depth change. The largest amounts of erosion (< 2.3 m) were measured on the southwest flank of the Boulder Patch area, west of Foggy Island Bay, but this area mostly had moderate and low erosion (n= 1,526, $\bar{x}$ = 0.40 m, ± 0.40; Figure 3A(b)), and there was little noteworthy offshore erosion. The highest amounts of deposition (>1.5 m) were measured just landward of the Narwhal/ Jeanette/ McClure barrier island chain located northeast of the survey tracklines but most of these depth change

comparisons (321 out of 521, or 62%) only showed moderate to low, and highly variable, deposition (n= 521, $\bar{x}$ = -0.25 m, ± 0.65; Figure 3A(c)).

The UAF 2018 survey of Stefansson Sound's Boulder Patch is not as spatially dense as the 1997 survey but extends farther west to Cross Island and east to the Newport Entrance. Similar to the 1997 results, a spatial trend in bathymetric change is apparent. The UAF 2018 data show consistent (2,883 out of 3,567 or 81%) but low deposition of less than one SD, and therefore within the bounds of uncertainty, east of the Boulder Patch (n= 3,567, $\bar{x}$ = -0.14 m, ± 0.18; Figure 3B(a)), where the 1997 data showed no depth change. The single transect from 2018 that bifurcates the larger boulder patch (n= 1,201, $\bar{x}$ = 0.14 m, ± 0.27; Figure 3B(b)) indicates a change from slight erosion in 1997 to neutral depth change across the lower density 'light' boulder patch area (n= 692, $\bar{x}$ = 0.05 m, ± 0.21), whereas no change in the erosion from 1997 appears to have occurred across the small region of 'heavy' high-density boulders (n= 509, $\bar{x}$ = 0.26 m, ± 0.30; Figure 3B(b)). The channel between the two larger boulder patches also appears to have switched from low erosion in 1997 to neutral depth change in 2018 (n= 1,379, $\bar{x}$ = 0.03 m, ± 0.22; Figure 3B(c)). A larger area of high deposition (908 of 1,527 observations or 59% > 1 m) than observed in 1997 was measured landward of the Narwhal/ Jeanette/ McClure barrier islands (n= 1,527, $\bar{x}$ = -1.26 m, ± 0.88; Figure 3B(d)), and the expanded footprint of the 2018 data showed this high deposition extended west to Dinkum Sands, and Cross and Bartlett islands. The highest deposition (n= 654, $\bar{x}$ = -2.29 m, ± 1.18) in the Dinkum Sands region amounts occur immediately to the west of the area of the high erosion (n= 391, $\bar{x}$ = 1.90 m, ± 0.76; Figure 3B(e)). These seafloor changes associated with the barrier islands and Dinkum Sands are similar to the shoreline change observations of Gibbs and Richmond (2015; 2017), who determined that the narrow Stefansson Sound area barrier islands, often < 100 m wide, eroded and migrated

landward on average 420 m between 1947 and 2010. The Narwhal/ Jeanette/ McClure island chain experienced the greatest erosion and land loss during that time, with only a small island area emergent in 2010, apparently supplying the sediment we observed settling along the northeast edge of the Boulder Patch by 2018. While no shoreline change calculations were conducted along much of the Stefansson Sound mainland coast due to the presence of extensive river deltas, there were relatively low amounts of shoreline erosion measured near the Kadleroshilik River, where retreat distances averaged 42 m, a tenth of the barrier island erosion, for the time period between 1947 and 2010 (Gibbs and Richmond 2015; 2017).

3.3 Barter Island region

There are several regions of uniform seafloor erosion and deposition along the Arey and Barter island coasts, with erosion along more north-facing shorelines and deposition along more west-facing shorelines, generally matching the prograding and retreating patterns observed in the shorelines (Figure 4). Along the northeast-facing shore of Arey Island, which shows extreme retreat up to nearly 15 m/yr (Gibbs and Richmond 2017), sounding comparisons are all highly erosional in a contiguous area, shown roughly by the oval, ranging up to a 3.9 m increase in depth (n=1,177, $\bar{x}$ = 1.93 m, ± 0.77; Figure 4(a)). Immediately to the west of the region of seafloor erosion, west of the apex of Arey Island, where the shoreline faces northwest and shoreline change becomes accretional, is a seafloor area showing uniformly high deposition in a contiguous area roughly shown with the oval, as high as 3.2 m (n=2,111, $\bar{x}$ = -1.62 m, ± 0.44) (Figure 4(b)). This pattern of adjacent seafloor erosion and deposition is repeated along the western end of Barter Island, with the small number of the shallowest (< 4 m), inshore depth comparisons all showing erosion of up to 2.3 m along a low to moderately retreating shoreline (n=74, $\bar{x}$ =1.09 m, ±0.56; Figure 4(c)), right next to a west-facing prograding shore, and adjacent

foreshore exhibiting mostly low to moderate (< 1.6 m) deposition (n= 503, $\bar{x}$ =-0.99 m, ±0.25; Figure 4(d)). Inside Arey Lagoon, in the vicinity of the narrow inlet between the eastern flank of Arey Island and the west spit attached to Barter Island, mostly low to moderate erosion (< 1.0 m) was observed (n= 6,274, $\bar{x}$ = 0.31 m, ±0.17; Figure 4(e)). Offshore and to the northwest of Arey Island is a region of mostly low deposition (< 0.8 m) from multibeam survey D00168, in depths ranging from about 11 to 13 m (n=24, $\bar{x}$ =-0.19 m, ±0.24; Figure 4(f)).

3.4 Currents

Maximum bottom currents exceed 200 cm/s (Figure 6A) along the west-facing coast of Point Barrow on the Chukchi side. These strong currents are associated with bathymetric steering of Pacific waters flowing northward through the Bering Strait across the Chukchi Sea and along the Barrow Canyon (Gong and Pickart, 2015; Pickart et al., 2016; Weingartner et al., 2017). Previous studies (e.g., Weingartner et al., 1998; Pickart et al., 2005; Itoh et al., 2013; Fang et al., 2017) have shown that variations in water transport and currents are primarily wind-forced and vary seasonally and in-phase with the annual cycle of Bering Strait transport with minima and maxima occurring in winter and summer, respectively. Extraneous to this region of deep but near-coast strong currents, maximum bottom currents are substantially slower. Maximum bottom currents on the northeast-facing side of Point Barrow and within Elson Lagoon are on the order of 30 cm/s and 15 cm/s, respectively. Within Stefansson Sound and Foggy Island Bay, maximum currents are <50 cm/s, while at Barter Island and within Arey Lagoon maximum currents are on the order of 30 cm/s and 10 cm/s, respectively. Because we are not privy to model results and observations that are coincident in time, a robust model validation for the specific regions of interest to this study is not possible, but comparison between modeled maximum bottom currents in 2015 tend to be biased low by ~-25% compared to observations obtained in 1999-2000 near

Foggy Island Bay (maximum measured currents of 65 cm/s at McClure by Weingartner et al. 2009), and ~-50% compared to observations collected in 2011 near Barter Island and Arey Lagoon (Erikson et al., 2020).

Comparing computed bed shear stresses using U100 values at the closest model grid point to usSEABED (Buczkowski et al., 2020a; 2020b; Figure 6B-D) sediment sample locations (Eq. 1) and comparing these to the critical shear stress (Eq. 2), the solid line in Figure 6E shows that the majority of the sediment samples analyzed can be mobilized and transported by tidal, geostrophic, and atmospheric driven currents (72% of the Utqiagvik samples, and 92% of the Stefansson Sound samples). The single sediment sample within the Barter Island study area falls below the critical threshold for incipient motion but as noted above, the model appears to be biased low and with only a single seabed sediment sample, it is not possible to infer if oceanic currents impart changes of the seabed.

3.5 Waves

The annual mean inner depths-of-closure (Eq. 3a; h_{in}) are similar at all sites, ranging between 2.90 and 3.20 m (Table 3). Only at Utqiagvik was a statistically significant (*p-value*<0.05) trend of increasing h_{in} found (0.03m/yr). In contrast, outer depths-of-closure (Eq. 3b; h_{out}) were found to be statistically significant at all three sites during the reanalysis period of 1979 to 2019, indicating an increasing capacity for seafloor impacts (Table 3). Deepest h_{out} (9.3 ± 2.9 m) were found to occur at Utqiagvik, followed by Barter Island (7.0 ± 1.7 m), and slightly shallower Stefansson Sound (6.2 ± 1.9 m) (Figure 7; Table 3). The h_{out} values in the vicinity of Utqiagvik indicate that cross-shore wave processes are likely responsible for observed changes along the northeast-facing spit immediately east of Point Barrow. Furthermore the observed erosion-deposition-erosion pattern may be a reflection of cross-shore bar movement that is typical of many beaches (Short, 1973; 1975). Within Elson Lagoon, in the vicinity of Utqiagvik,

which is protected from direct open coast wave energy, much of the change cannot be attributed to cross-shore processes by open ocean developed wind-waves (locally generated waves may still impact the seabed). In Stefansson Sound much of the observed erosion and deposition is within the bounds of the DOC (Figure 5B and landward bound of gray shading in Figure3A&B). Deposition within the DOC region is primarily concentrated along the east margins of Foggy Island Bay and may reflect dampening of wave energy that would allow for sediment to settle and deposit in the shadows of the Boulder Patch and barrier islands. Along the open coast of Barter Island, much of the observed seabed change is within h_{in} (points in water depths < 3.2 ± 0.7 m, Figure 4 and 5C), suggesting that waves are a dominant mechanism for entrainment and transport of sediment along this section of coast. Similar to Elson Lagoon, no conclusions can be made of wave-induced transport within Arey Lagoon since local wave growth within the lagoons is not evaluated here.

5. Discussion

5.1 Indicators of physical drivers – resuspension and transport

This is one of the first studies to quantify patterns of nearshore erosion and deposition using *in situ* measurements along Alaska's Beaufort Sea coast, an area well known for recent, significant shoreline change (Brown et al., 2003; Mars and Houseknecht, 2007; Jones et al., 2009; Tweedie et al., 2012; Gibbs and Richmond, 2015; 2017; Jones et al., 2018). By carefully correcting the post-WWII smooth sheet soundings, an often misunderstood resource of historical seafloor observations, we showed that there was a spatial link between the previously documented shoreline erosion/progradation of Gibbs and Richmond (2015; 2017) and nearby seafloor erosion/deposition. We also showed that relatively uniform regions of seafloor depth change may alternate between erosion and deposition off of the same section of shoreline, and

that these regions of relatively uniform seafloor depth change may occur up to about 5 km from the shoreline. In general, the observed bathymetric change can be attributed to coastal currents driven by wind-stress, atmospheric pressure gradients, large-scale quasi-steady water surface slopes and horizontal density gradients associated with oceanic circulations and waves as indicated by comparing measured sediment characteristics with current velocity outputs from a 3D numerical model and wave conditions from an earth-systems reanalysis product. Our analysis shows that these well-known forces of coastal change demonstrate greater complexity offshore, as revealed in the two-dimensional patterns of change in the offshore environment. While not evaluated here, it is also well known that sea-ice related processes (such as ice-gouging) can significantly alter the seabed (Barnes et al., 1984) but also that tidal currents are small in this region and provide insignificant modes of transport except in the case of very fine cohesive sediment (Baumann et al., 2020).

Using simple metrics, we have shown that sediment resuspension and transport by both wave and non-wave driven currents landward of the ~13 m isobath and outside of Elson and Arey Lagoons likely contribute to the overall patterns of observed change at all three studied sites (within the 9.3 ± 2.9 m, 7.0 ± 1.7 m, and 6.2 ± 1.9 m isobaths at Utqiagvik, Barter Island, and Stefansson Sound, respectively). These findings are supported by previous observation and modeling studies (Aumack et al., 2007; Coastal Frontiers Corporation, 2014; Bonsell and Dunton, 2018; Erikson et al., 2020).

Within Elson Lagoon, Stierle and Eicken (2002) showed that bottom sediment resuspension varies temporally and spatially and is controlled by local bathymetry and interannually by wind velocity and fetch. Along the open coast and east of Point Barrow, where our results showed deposition on the Chukchi side (west) of Point Barrow and more complicated

patterns of erosion and deposition east of Point Barrow, the results are generally consistent with survey results reported by Hume and Schalk (1967). Based on repeat surveys begun in 1958, Hume and Schalk documented southeastward transport of sediment and a 20-fold increase in transport associated with the extreme storm of 1963. A complex pattern of bathymetrically steered geostrophic strong currents combined with intermittent storm waves and wind-driven currents appear responsible for the overall observed change (Gong and Pickart, 2015; Pickart et al., 2016; Fang et al., 2017; Weingartner et al., 2017).

Driven by the need to document changes potentially associated with the construction of oil and gas exploration infrastructure, extensive measurements of total suspended sediment concentrations throughout Stefansson Sound date back to the early 1980s (USACE, 1984). Measurements show strong correlations between increasing wind speed and increasing suspended sediment concentrations during the ice-free season, presumably from resuspension of bottom sediments (Trefry et al., 2009). Detailed sediment transport modeling substantiates measured deposition patterns around the Endicott Causeway between 1989 and 2009/10 (Yager, 2011). The deposition patterns surrounding the causeway were variable with depth changes up to ~1 m over the ~20-year period, save one small patch with exceptionally high deposition near the terminus of the causeway.

As part of a study to evaluate future flood patterns and stability of Arey Island, with respect to sea-level rise and changing storm conditions, Erikson et al. (2020) derived hindcast (1981 to 2010) and future (2011 to 2100) conditions of open-water season wave conditions, currents, and morphologic change using a suite of numerical models. Model simulations of sediment transport and morphologic change, driven by waves, tides, and storm surge, were found to be sufficiently strong to transport sediment presently available within the nearshore and on the

barrier islands. Model results of past conditions corroborate the findings of this study in that the western portion of Arey Island has been relatively stable while the eastern portion was highly dynamic. The pattern of a highly dynamic eastern portion and relatively stable western portion of the island was found to continue into the future, assuming unchanging sediment supply.

5.2 Sediment sources

Whereas large amounts of resuspended sediment, driven by waves and currents, are transported across and along the inner nearshore zone and likely responsible for much of the observed change, sediment flux from streams and eroding bluffs are major contributors to the overall sediment budgets and bathymetric change. The Sagavanirktok River, one of the three largest rivers that drain Alaska's North Slope, terminates in Stefansson Sound with an approximate annual water discharge of 1.6 km^3/yr (McClelland, 2014). Adjacent to Arey Lagoon are the Hulahula River (0.5 km^3/yr) (Stuefer et al., 2017) and the much smaller Okpilak River. The Sagavanirktok, Hulahula and Okpilak rivers originate in the Brooks Range where they drain snowfields and glaciers and subsequently journey across the tundra, eventually reaching the coast to release organic and non-organic silts and fine to medium sands (Lock et al., 1989). While these sediment loads are reasonably large, major, distant rivers such as the Colville and Mackenzie also provide sediment that transport alongshore contributing to the overall sediment budget and bathymetric change, far beyond the locations where they enter the Beaufort Sea (e.g., Dunton et al., 1982).

Similar to influx of riverine sediment loads, material flux from eroding bluffs contribute to shoreline and bathymetric changes both locally and distally from the originating source. Along the open coast of Barter Island, Gibbs et al. (2019a) observed deposition of eroded bluff material at the base of the bluff and subsequent removal of the debris apron. During a single year

(2014/2015), the bluffs experienced a net volume loss of 38,100 ± 300 m^3 (1.3 m^3 per meter of shoreline) and, although very episodic, the volumetric loss was found to be similar to the long-term annual average computed over 1955-2015 (Gibbs et al., 2019a). Erosion rates and volumetric material flux are variable across the Alaska Beaufort Sea coast. Along the mainland of Stefansson Sound, insignificant bluff recession and material flux have occurred, possibly due in part to the protection of shore-aligned barrier islands that mitigate wave impacts on the mainland shore. At the west end of our study area at Elson Lagoon, where fetch is sufficiently large to generate waves and the bluffs are primarily made up of fine sediment, volumetric losses averaged 0.8-3.5 m^3/m/yr from 2003 to 2015 (Tweedie et al., 2016).

Inferences between eroded bluff material and changes in nearshore bathymetry can, to some degree, be made at the three study sites investigated here. For example, the east-west trending spit at Barter Island and infilling of the inlet between Arey Island and the spit are likely the result of both eroded bluff material and resuspended sediment transported alongshore. Bluff material at Barter Island is comprised of fine to medium sand and gravel (Erikson et al., 2020), making it both suitable for transport and deposition nearby and further from the originating source. In contrast, eroded bluff material from Elson Lagoon bluffs is likely to remain within the lagoon due to the semi-enclosed geography, and is reflected in the eroding shoreline and depositional environment of the lagoon (Figure 2).

5.3 Implications for the future

The magnitude to which the nearshore bathymetry will continue to change (increase/decrease in depth) depends on future ocean conditions (storms, sea ice), delivery of volumes of sediment, and their characteristics. The frequency and magnitude of wave energy and storm surges appear to be increasing (Atkinson, 2005; Casas-Prat and Wang, 2020; Erikson et

al., 2020), as are sediment influxes from rivers (Hobson, 2006) and eroding bluffs (Jones et al., 2008; Gibbs et al., 2021). Field studies on shallow, depth-dependent species along the Beaufort Sea coast would benefit from the incorporation of trends in bathymetric change identified in this study when considering climate change impacts. Exposure or burying of sessile infauna may be significant in some areas, more mobile epifauna may avoid or colonize newly surfaced seafloor areas, and fish may shift their ontogenetic and seasonal migrations. For example, the shallowing of central and northern Elson Lagoon, along with the deepening in its western area and eastern entrance, may change the distribution of abundant fish species such as least cisco (*Coregonus sardinella*), fourhorn sculpin (*Myoxocephalus quadricornis*), and juvenile pink (*Oncorhynchus gorbuscha*) and chum (*O. keta*) salmon (Logerwell et al., 2015). Outside of the lagoon but also in the Utqiagvik region, the nearshore and abundant species of capelin (*Mallotus villosus*) and Arctic cod (*Boreogadus saida*) (Logerwell et al., 2015) may follow retrograding barrier islands. In this study we show that the depth-of-closure, that is, the depth seaward of which there is no significant cross-shore sediment transport, has expanded and that with continued increases in wave heights and periods, bathymetric change will likely extend farther offshore with time. Because wave transformation to the nearshore is critically dependent on nearshore bathymetry, and bluff erosion is critically dependent on nearshore wave conditions (Lantuit et al., 2012; Ravens et al., 2012; Barnhart et al., 2014; Fritz et al., 2017; Vincent et al., 2017; Bull et al., 2020; Frederick et al., 2021) there is a feedback cycle with respect to information needs required to predict shoreline change and consequent adverse impacts on coastal infrastructure, habitats, and communities. Increasing loads of sediment from rivers and bluffs to the nearshore coastal system could offset the expanding depth-of-closure and moreover are likely to change the dynamic evolution (including beaches, spits, barrier islands) of the coastline. However, projections of

these processes are still poorly quantified and thus warrant more in-depth further studies. Additionally, the majority of the nearshore Alaskan Beaufort Sea coast was last surveyed more than 70 years ago, as exemplified in the limited geographic scope of the study presented herein; thus, there is a need to not only update nearshore bathymetric measurements from the legacy post-WWII soundings, but also to perform repeat surveys in the coming decades, particularly in areas of rapid change and of greatest concern.

6. Conclusions

Seasonal variations in hydrodynamics and sediment supply control sediment transport and bathymetric change. In this study, we evaluated bathymetric change where single- or multibeam bathymetry have been collected within recent decades and overlap with the otherwise most comprehensive nearshore bottom surveys across the Alaska Beaufort Sea from the post-WWII era. Existing data coverage limited this study to three regions at the west, central, and east ends of the Alaska Beaufort coast: Point Barrow and Elson Lagoon, Stefansson Sound, and the vicinity of Barter Island. Our limited depth comparisons show the value of this approach for better understanding coastal change processes and supports expanding this type of analysis as more nearshore bathymetry data are collected.

Relevant to the observed bathymetric changes are sea-ice related processes such as ice scour, resuspension and transport of seabed and shoreline sediment, and additionally the availability and influx of sediment to the nearshore coastal system from sediment-laden river flows and eroding bluffs. Whereas ice scour can substantially rework the seabed along individual track lines like those analyzed here, these actions produce highly variable seafloor depth change rather than the fairly uniform depth changes that we observed. Instead, sediment resuspension and transport likely contribute to the overall patterns of change. Identifying littoral cells and

estimating sediment budgets for the investigation into all processes that contribute to the observed depth changes are beyond the scope of this study and not feasible due to the lack of data. However, indications are that sediment loads from rivers and eroding bluffs have increased over the past decades and likely have contributed to the change (such as deposition within Elson Lagoon). Wave energy along the exposed coast has also increased, resulting in an expanding depth-of-closure that is deepening by 0.06 to 0.15 m/yr at the three study sites between 1979 and 2019 (Table 3). The balance between continued increases in wave energy and transport and deposition of sediment from both along and cross-shore processes will determine if the nearshore bathymetry changes will expand further offshore.

Ideally, a project such as ours would be conducted under carefully controlled and monitored conditions, but as ours is a retrospective analysis, we are utilizing available data sets, interpreted for our purposes, over uncontrolled periods. While we agree that it is unwise to place much weight on the exact quantitative depth changes of grouped observations reported here that are roughly equal to, or smaller than, the original units of depth measurement (1 ft or 0.305 m) and with large standard deviations, we also think that it is a mistake to disregard them completely. For example, the large (125 km^2) area of low (<0.5 m) deposition within Elson Lagoon, occurring between areas of higher deposition and areas of low to moderate erosion, is the result of thousands of depth change comparisons. We argue that its geographical placement and small depth change values makes more sense than assuming that some sort of depth sounding bias occurred only and consistently at this location.

The lack of permanent surface moorings collecting wind, wave, and current data in this area also hampered a direct analysis. While we are not directly measuring or modeling the movement of individual sediment particles, we are able to provide supporting information on

fluvial sediment loads, sediment types, seasonal sea ice extents, waves, and currents to illuminate possible drivers of sediment transport pathways and redistribution patterns for a better understanding the mechanisms through which the observed coastal changes may have occurred. But a clear need for new and continued monitoring and modeling are needed to fully understand the observed seabed changes.

Acknowledgments

Some of this research was supported by an International Science Fellowship grant from NOAA/NMFS's Office of Science & Technology, with some matching support from the Department of Geological Sciences, Stockholm University, Stockholm, Sweden. Additional support was provided by the U.S. Geological Survey Coastal Marine Geology Program. J. Kasper and P. Duvoy were supported by the U.S. Bureau of Ocean Energy Management through Cooperative Agreement M17AC00020 (UAF) for the project titled: 'Wave and Hydrodynamic Modelling Within the Nearshore Beaufort Sea'. Additional funding for J. Kasper was provided under NSF Award # 1656026 "LTER: Beaufort Sea Lagoons: An Arctic Coastal Ecosystem in Transition." Thanks to the staff at NCEI (National Centers for Environmental Information: http://www.ngdc.noaa.gov) for frequent assistance with smooth sheets. K. Rand, B. Riggle, W. Palsson, and Michael Martin provided helpful reviews. Hilcorp Alaska, LLC graciously provided access to the Coastal Frontiers 1997 and 2013 bathymetric data. G. Hearon and C. Leidersdorf with Coastal Frontiers Corporation facilitated transfer of this data and provided valuable insight into the region. The findings and conclusions in the paper are those of the author(s) and do not necessarily represent the views of the National Marine Fisheries Service or the U.S. Geological Survey. Any use of trade, product, or firm names in this publication is for descriptive purposes only and does not imply endorsement by the U.S. Government.

References

Alkire, M., Trefry, J.H., 2006. Transport of spring floodwater from rivers under ice to the Alaskan Beaufort Sea. J. Geophys. Res. 111.

Atkinson, D.E., 2005. Observed storminess patterns and trends in the circum-Arctic coastal regime. Geo-Marine Letters, 25(2-3), pp.98-109. https://doi.org/10.1007/s00367-004-0191-0

Aumack, C.F., Dunton, K.H., Burd, A.B., Funk, D.W. and Maffione, R.A., 2007. Linking light attenuation and suspended sediment loading to benthic productivity within an Arctic kelp-bed community 1. Journal of Phycology, 43(5), pp.853-863.

Baker, M.R., Palsson, W., Zimmermann, M., and Rooper, C.N. 2019. Model of trawlable area using benthic terrain and oceanographic variables - informing survey design and habitat maps in the Gulf of Alaska. Fisheries Oceanography, 28(6): 629-657. https://doi.org/10.1111/fog.12442

Barnes, P.W., Rearic, D.M., Reimitz, E. 1984. Ice gouging characteristics and processes. The Alaskan Beaufort Sea: Ecosystems and Environments eds. Barnes, Schell, and Remnitz. Academic Press, San Diego, pp.185-212.

Barnes, P.W. and Rearic, D.M., 1985. Rates of sediment disruption by sea ice as determined from characteristics of dated ice gouges created since 1975 on the inner shelf of the Beaufort Sea, Alaska. US Department of the Interior, Geological Survey.

Barnhart, K.R., Anderson, R.S., Overeem, I., Wobus, C., Clow, G.D. and Urban, F.E., 2014. Modeling erosion of ice-rich permafrost bluffs along the Alaskan Beaufort Sea coast. Journal of Geophysical Research: Earth Surface, 119(5), pp.1155-1179, doi:10.1002/2013JF002845.

Baumann, T. M., I. V. Polyakov, L. Padman, S. Danielson, I. Fer, M. Janout, W. Williams and A. V. Pnyushkov (2020). Arctic tidal current atlas. Scientific Data 7(1): 275.

Biskaborn, B. K., Smith, S.L., Noetzli, J., Matthes, H., Vieira, G., Streletskiy, D.A., Schoeneich, P., Romanovsky, V.E., Lewkowicz, A.G., Abramov, A. and Allard, M., 2019. Permafrost is warming at a global scale. Nat. Commun. 10, 2017–2019.

Bonsell, C. and Dunton, K.H., 2018. Long-term patterns of benthic irradiance and kelp production in the central Beaufort sea reveal implications of warming for Arctic inner shelves. Progress in Oceanography, 162, pp.160-170.

Brown, J., Jorgenson, M.T., Smith, O.P. and Lee, W., 2003, July. Long-term rates of coastal erosion and carbon input, Elson Lagoon, Barrow, Alaska. In Eighth International Conference on Permafrost (Vol. 21, p. 25). Retrieved from http://research.iarc.uaf.edu/NICOP/DVD/ICOP 2003 Permafrost/Pdf/Chapter_019.pdf

Buczkowski, B.J., Reid, J.A., and Jenkins, C.J., 2020a. Sediments and the sea floor of the continental shelves and coastal waters of the United States—About the usSEABED integrated sea-floor-characterization database, built with the dbSEABED processing system: U.S. Geological Survey Open-File Report 2020–1046, 14 p., https://doi.org/ 10.3133/ ofr20201046.

Buczkowski, B.J., Reid, J.A., Schweitzer, P.N., Cross, V.A., and Jenkins, C.J., 2020b. usSEABED—Offshore surficial-sediment database for samples collected within the United States Exclusive Economic Zone: U.S. Geological Survey data release, https://doi.org/10.5066/P9H3LGWM.

Bull, D.L.,E. M. Bristol, E. Brown, R. C. Choens, C. T. Connolly, C. Flanary, J. M. Frederick, B. M. Jones, C. A. Jones, M. Ward Jones, J. W. McClelland, A. Mota, I. Tezaur

(2020). Arctic Coastal Erosion: Modeling and Experimentation, SAND2020-10223, Sandia National Laboratories, NM.

Buster, N.A., and Morton, R.A., 2011. Historical bathymetry and bathymetric change in the Mississippi-Alabama coastal region, 1847–2009: U.S. Geological Survey Scientific Investigations Map 3154, 13 p. pamphlet.

Calder, B., 2006. On the uncertainty of archive hydrographic data sets. IEEE Journal of Oceanic Engineering, 31(2), pp.249-265.

Casas-Prat, M. and Wang, X.L., 2020. Projections of extreme ocean waves in the Arctic and potential implications for coastal inundation and erosion. Journal of Geophysical Research: Oceans, 125(8), p.e2019JC015745.

Coastal Frontiers Corporation, 2014. Suspended sediment dispersal during the Liberty Development construction. Prepared for BP Exploration, Anchorage, AK. Report pub. Moorpark, CA. 60 pp.

Conlan, K.E. and Kvitek, R.G., 2005. Recolonization of soft-sediment ice scours on an exposed Arctic coast. Marine Ecology Progress Series, 286, pp.21-42.

Copernicus Climate Change Service (C3S) 2017: ERA5: Fifth generation of ECMWF atmospheric reanalyses of the global climate. Copernicus Climate Change Service Climate Data Store (CDS), date of access. https://cds.climate.copernicus.eu/cdsapp#!/home

Curchitser, E.N., K. Hedstrom, S. Danielson and J. Kasper, 2017. Development of a very high-resolution regional circulation model of Beaufort Sea nearshore areas. Anchorage, AK, U.S. Department of the Interior, Bureau of Ocean Energy Management, Alaska OCS Region: 81.

Danek, L., and Tourtellotte, G., 1987. 1985 Final Report for the Endicott Environmental Monitoring Program, Volume V: Sedimentation and Erosion Monitoring. Prepared by Envirosphere Corporation for U. S. Army Corps of Engineers, Alaska District.

Dunton, K.H., E. Reimnitz, and S. Schonberg. 1982. An Arctic Kelp Community in the Alaskan Beaufort Sea. Arctic 465-484.

Erikson, L.H., Gibbs, A.E., Richmond, B.M., Jones, B.M., Storlazzi, C.D., and Ohman, K.A., 2020. Modeled 21st century storm surge, waves, and coastal flood hazards, and supporting oceanographic and geological field data (2010 and 2011) for Arey and Barter Islands, Alaska and vicinity: U.S. Geological Survey data release, https://doi.org/10.5066/P9LGYO2Q

Fang, Y.-C., R.A. Potter, H. Statscewich, T.J. Weingartner, P. Winsor and B.K. Irving, 2017. Surface current patterns in the northeastern Chukchi Sea and their response to wind forcing. Journal of Geophysical Research: Oceans 122(12): 9530-9547.

Frederick, J., Mota, A., Tezaur, I. and Bull, D., 2021. A thermo-mechanical terrestrial model of Arctic coastal erosion, Journal of Computational and Applied Mathematics, doi: https://doi.org/10.1016/j.cam.2021.113533.

Fritz, M., Vonk, J.E. and Lantuit, H., 2017. Collapsing arctic coastlines. Nature Climate Change, 7(1), pp.6-7.

Gibbs, A.E., Richmond, B.M., 2015. National assessment of shoreline change—Historical shoreline change along the north coast of Alaska, U.S.–Canadian border to Icy Cape: U.S. Geological Survey Open-File Report 2015–1048, 96 p., http://dx.doi.org/10.3133/ofr20151048.

Gibbs, A.E., Richmond, B.M., 2017. National assessment of shoreline change—Summary statistics for updated vector shorelines and associated shoreline change data for the

north coast of Alaska, U.S.-Canadian border to Icy Cape: U.S. Geological Survey Open-File Report 2017–1107, 21 p., https://doi.org/10.3133/ofr20171107.

Gibbs, A.E., Nolan, M., Richmond, B.M., Snyder, A.G. and Erikson, L.H., 2019a. Assessing patterns of annual change to permafrost bluffs along the North Slope coast of Alaska using high-resolution imagery and elevation models. Geomorphology, 336, pp.152-164.

Gibbs, A.E., Snyder, A.G., Richmond, B.M., 2019b, National assessment of shoreline change - Historical shoreline change along the north coast of Alaska, Icy Cape to Cape Prince of Wales: U.S. Geological Survey Open-File Report 2019-1146, 52 p., https://doi.org/10.3133/ofr20191146

Gibbs, Ann E., Li H. Erikson, Benjamin M. Jones, Bruce M. Richmond, and Anita C. Engelstad 2021. Seven Decades of Coastal Change at Barter Island, Alaska: Exploring the Importance of Waves and Temperature on Erosion of Coastal Permafrost Bluffs. *Remote Sensing* 13, no. 21: 4420. https://doi.org/10.3390/rs13214420

Gong, D., and Pickart, R.S. 2015. Summertime circulation in the eastern Chukchi Sea. Deep Sea Research Part II: Topical Studies in Oceanography, 118, 18– 31. https://doi.org/10.1016/j.dsr2.2015.02.006

Hachmeister, L.E., Short, K.S., Schrader, G.C., Winnick, K.B., and Johannessen, J.W., 1985. Oceanographic Monitoring. Endicott Environmental Studies. Envirosphere Company, Bellevue, WA.

Hallermeier, R.J. 1981. A Profile Zonation for Seasonal Sand Beaches from Wave Climate. Coastal Engineering, Vol. 4, 253-277.

Hallermeier, R.J. 1983. Sand transport limits in coastal structure design, pp. 703-716. *In* Proceedings, Coastal Structures ’83, American Society of Civil Engineers.

Hearon, G., D. Dickins, K. Ambrosius, and K. Morris. 2009. Mapping Sea Ice Overflood Using Remote Sensing: Smith Bay to Camden Bay. Report prepared by DF Dickins Associates, Coastal Frontiers Corporation, Aerometric, and The Geophysical Institute, University of Alaska for US Department of Interior, Minerals Management Service, Alaska OCS Region under Contract M06PC00034.

Hobson, A.C.H., 2006. Using remotely-sensed nearshore suspended sediment as an indicator of environmental change on the Alaskan North Slope. University of Colorado at Boulder. *Ph. D. Thesis*.

Horowitz, W., 2002. Evaluation of Sub-Sea Physical Environmental Data for the Beaufort Sea OCS and Incorporation into a Geographic Information System (GIS) Database. OCS Study MMS 202-017. 76 pp.

Hume, J.D. and Schalk, M., 1967. Shoreline processes near Barrow, Alaska: a comparison of the normal and the catastrophic. Arctic, pp.86-103.

Itoh, M., Nishino, S., Kawaguchi, Y. and Kikuchi, T., 2013. Barrow Canyon volume, heat, and freshwater fluxes revealed by long-term mooring observations between 2000 and 2008. Journal of Geophysical Research: Oceans, 118(9), pp.4363-4379.

Jakobsson, M., Mayer, L.A., Bringensparr, C., Castro, C.F., Mohammad, R., Johnson, P.,... & Zinglersen, K. B, 2020. The international bathymetric chart of the Arctic Ocean version 4.0. Scientific data, 7(1), pp.1-14.

Jones, B.M., Hinkel, K.M., Arp, C.D. and Eisner, W.R., 2008. Modern erosion rates and loss of coastal features and sites, Beaufort Sea coastline, Alaska. Arctic, pp.361-372.

Jones, B.M., Arp, C.D., Jorgenson, M.T., Hinkel, K.M., Schmutz, J.A. and Flint, P.L., 2009. Increase in the rate and uniformity of coastline erosion in Arctic Alaska. Geophysical Research Letters, 36(3). https://doi.org/10.1029/2008GL036205

Jones, B.M., Farquharson, L.M., Baughman, C.A., Buzard, R.M., Arp, C.D., Grosse, G., Bull, D.L., Günther, F., Nitze, I., Urban, F. and Kasper, J.L., 2018. A decade of remotely sensed observations highlight complex processes linked to coastal permafrost bluff erosion in the Arctic. Environmental Research Letters, 13(11), p.115001. https://doi.org/10.1088/1748-9326/aae471

Kasper, J., Jump, S., and Duvoy, P., 2019. Central Beaufort Sea wave and hydrodynamic modeling study 2018 Field Report to the Bureau of Ocean Energy Management, UAF Cooperative Agreement M17AC00020/USGS Intra-agency Agreement M17PG00046.

Kraus, N.C., Larson, M. and Wise, R.A. 1998. Depth of Closure in Beach-fill Design, Coastal Engineering Technical Note CETN II-40, 3/98, U.S. Army Engineer Waterways Experiment Station, Vicksburg, MS.

Kumar, A., J. Yadav, and Mohan, R. 2020. Global warming leading to alarming recession of the Arctic sea-ice cover: Insights from remote sensing observations and model reanalysis. Heliyon 6(7): e04355.

Laman, E.A., Rooper, C.N., Rooney, S.C., Turner, K.A., Cooper, D.W., and Zimmermann, M. 2017. Model-based essential fish habitat definitions for Bering Sea groundfish species. U.S. Dep. Commer., NOAA Tech. Memo. NMFS-AFSC-357, 265 p.

Lantuit, H., Overduin, P.P., Couture, N., Wetterich, S., Aré, F., Atkinson, D., Brown, J., Cherkashov, G., Drozdov, D., Forbes, D.L. and Graves-Gaylord, A., 2012. The Arctic coastal dynamics database: a new classification scheme and statistics on Arctic permafrost coastlines. Estuaries and Coasts, 35(2), pp.383-400. https://doi.org/10.1007/s12237-010-9362-6

Latapy, A., Héquette, A., Pouvreau, N., Weber, N. and Robin-Chanteloup, J.B., 2019. Mesoscale morphological changes of nearshore sand banks since the early 19th century, and their influence on coastal dynamics, Northern France. Journal of Marine Science and Engineering, 7, 73. doi:10.3390/jmse7030073

Laurel, B.J., Copeman, L.A., Spencer, M. and Iseri, P., 2017. Temperature-dependent growth as a function of size and age in juvenile Arctic cod (*Boreogadus saida*). ICES Journal of Marine Science, 74(6), pp.1614-1621. https://doi.org/10.1093/icesjms/fsx028

Leffingwell, E. de K., 1908. Flaxman Island, A Glacial Remnant. Journal of Geology, (6)1, pp. 56-64.

Lim, M., Whalen, D., Mann, P.J., Fraser, P. and Berry, H.B., 2020. Effective monitoring of permafrost coast erosion : Wide-scale storm impacts on outer islands in the Mackenzie Delta area. Front. Earth Sci. 8, 1–17.

Lock, M.A., Ford, T.E., Fiebig, D.M., Miller, M.C. and Hullar, M., 1989. Biogeochemical survey of rivers and streams in the mountains and foot-hills province of arctic Alaska. Archiv fuer Hydrobiologie AHYBA 4, 115(4).

Logerwell, E., Busby, M., Carothers, C., Cotton, S., Duffy-Anderson, J., Farley, E., Goddard, P., Heintz, R., Holladay, B., Horne, J. and Johnson, S., 2015. Fish communities across a spectrum of habitats in the western Beaufort Sea and Chukchi Sea. Progress in Oceanography, 136, pp.115-132.

Mahoney, A., Eicken, H. and Shapiro, L., 2007. How fast is landfast sea ice? A study of the attachment and detachment of nearshore ice at Barrow, Alaska. Cold Regions Science and Technology, 47(3), pp.233-255.

Mars, J.C., and Houseknecht, D.W., 2007. Quantitative remote sensing study indicates doubling of coastal erosion rate in past 50 yr along a segment of the Arctic coast of Alaska. Geology, v.35, no. 7; p. 583-586.

Martin, L.R., and Gallaway, B.J., 1994. The effects of the Endicott Development Project on the Boulder Patch, an Arctic kelp community in Stefansson Sound, Alaska. Arctic. 47(1): 54-64.

Martin, P.J., Edwards, K.L., Hebert, D.A. and Allard, R.A., 2015. Implementation of Wetting and Drying in NCOM: Description and Validation Test Report. Naval Research Lab Stennis Detachment, Stennis Space Center MS Ocean Dynamics and Prediction Branch.

McClelland, J.W., A. Townsend-Small, R.M. Holmes, F. Pan, M. Stieglitz, M. Khosh, and B.J. Peterson. 2014. River export of nutrients and organic matter from the North Slope of Alaska to the Beaufort Sea, Water Resour. Res., 50, 1823–1839, doi:10.1002/2013WR014722.

National Oceanic and Atmospheric Administration (NOAA), 2021. Tides and Currents—Prudhoe Bay, AK—Station ID 9497645. Available online: http://tidesandcurrents.noaa.gov/stationhome.html?id=9497645 (accessed on 28 January 2021)

Nederhoff, K., Erikson, L., Engelstad, A., Bieniek, P. and Kasper, J., 2021. The effect of changing sea ice on nearshore wave climate trends along Alaska's central Beaufort Sea coast. The Cryosphere Discussions, pp.1-33.

Overeem, I., Anderson, R.S., Wobus, C.W., Clow, G.D., Urban, F.E. and Matell, N., 2011. Sea ice loss enhances wave action at the Arctic coast. Geophysical Research Letters, 38(17).

Overland, J., Dunlea, E., Box, J.E., Corell, R., Forsius, M., Kattsov, V., Olsen, M.S., Pawlak, J., Reiersen, L.O. and Wang, M., 2019. The urgency of Arctic change. Polar Science, 21, pp.6-13.

Pickart, R.S., Weingartner, T.J., Pratt, L.J., Zimmermann, S. and Torres, D.J., 2005. Flow of winter-transformed Pacific water into the Western Arctic. Deep Sea Res., Part II, 52, 3175-3198.

Pickart, R.S., Moore, G.W.K., Mao, C., Bahr, F., Nobre, C., and Weingartner, T.J., 2016. Circulation of winter water on the Chukchi shelf in early summer. Deep Sea Research Part II: Topical Studies in Oceanography, 130, 56– 75. https://doi.org/10.1016/j.dsr2.2016.05.001

Ravens, T.M., Jones, B.M., Zhang, J., Arp, C.D. and Schmutz, J.A., 2012. Process-based coastal erosion modeling for drew point, North Slope, Alaska. Journal of Waterway, Port, Coastal, and Ocean Engineering, 138(2), pp.122-130. https://doi.org/10.1061/(ASCE)WW.1943-5460.0000106

Rearic, D.M., 1986. Estimates of sea ice energy expenditure on the seafloor of the Beaufort Sea, Alaska. In International offshore mechanics and arctic engineering. Symposium. 5 (pp. 589-592).

Rearic, D.M. and Ticken, E.J., 1988. Ice gouge processes in the Alaskan Beaufort Sea. Technical Council on Cold Regions Engineering Monograph, pp.85-107.

Reimnitz, E., and Barnes, P.W., 1974. Sea ice as a geologic agent on the Beaufort Sea Shelf of Alaska. Symposium on Beaufort Sea Coastal and Shelf Research: January 7, 8 & 9, 1974, San Francisco, CA.: Program, abstracts, theme papers, Arctic Institute of North America, Arlington, VA, 301-351.

Reimnitz, E. and Kempema, E.W., 1983. High rates of bedload transport measured from infilling rate of large strudel-scour craters in the Beaufort Sea, Alaska. Continental Shelf Research, 1(3), pp.237-251.

Richter-Menge, J. and Druckenmiller, M.L. 2020. The Arctic. *In* State of the Climate in 2019. (eds. Diamond, H. J. & Schreck, C. J.) 101, 185-S238 (Bulletin of the American Meteorological Society).

Rooney, S., Rooper, C.N., Laman, E.A., Turner, K., Cooper, D., Zimmermann, M. 2018. Model-based Essential Fish Habitat Definitions for Gulf of Alaska Groundfish Species. U.S. Dep. Commer., NOAA Tech. Memo. NMFS-AFSC-373, 370 p.

Rooper, C.N., Zimmermann, M., Prescott, M.M. and Hermann, A.J., 2014. Predictive models of coral and sponge distribution, abundance and diversity in bottom trawl surveys of the Aleutian Islands, Alaska. Marine Ecology Progress Series, 503, pp.157-176.

Rooper, C.N., Sigler, M.F., Goddard, P., Malecha, P., Towler, R., Williams, K., Wilborn, R. and Zimmermann, M., 2016. Validation and improvement of species distribution models for structure-forming invertebrates in the eastern Bering Sea with an independent survey. Marine Ecology Progress Series, 551, pp.117-130.

Short, A.D., 1973. Beach dynamics and nearshore morphology of the Alaskan Arctic coast. Doctoral Dissertation, Louisiana State University and Agricultural & Mechanical College, 140 pp.

Short, A.D., 1975. Offshore bars along the Alaskan Arctic coast. J. Geology, 82(2), p.209-221.

Short, K.S., C.D. Janzen, C.J. Van Zee, and D.J. Hanzlick, 1991. Oceanography. In: 1987 Final Report for the Endicott Environmental Monitoring Program, Volume 3, Part II, Chapter 3.

Prepared for by Envirosphere Company for the U.S. Army Corps of Engineers, Alaska District, Anchorage, AK.

Soulsby, R.L., 1983. The bottom boundary layer of shelf seas. *In* Elsevier oceanography series (Vol. 35, pp. 189-266). Elsevier.

Soulsby, R.L., 1997. Dynamics of Marine Sands: A Manual for Practical Applications. Thomas Telford Publications.

Soulsby, R.L. and Whitehouse, R.J.S., 1997. Threshold of sediment motion in coastal environments. In Pacific Coasts and Ports' 97: Proceedings of the 13th Australasian Coastal and Ocean Engineering Conference and the 6th Australasian Port and Harbour Conference; Volume 1 (p. 145). Centre for Advanced Engineering, University of Canterbury.

Stierle, A.P. and Eicken, H., 2002. Sediment inclusions in Alaskan coastal sea ice: spatial distribution, interannual variability, and entrainment requirements. Arctic, Antarctic, and Alpine Research, 34(4), pp.465-476.

Stuefer, S.L., Arp, C.D., Kane, D.L. and Liljedahl, A.K., 2017. Recent extreme runoff observations from coastal Arctic watersheds in Alaska. Water Resources Research, 53(11), pp.9145-9163. https://doi.org/10.1002/2017WR020567

Thomson, J., Fan, Y., Stammerjohn, S., Stopa, J., Rogers, W.E., Girard-Ardhuin, F., Ardhuin, F., Shen, H., Perrie, W., Shen, H. and Ackley, S., 2016. Emerging trends in the sea state of the Beaufort and Chukchi seas. Ocean Modelling, 105, pp.1-12.

Timmermans, M. L. and Ladd, C. 2019. Sea surface temperature, p. 754–759. *In* Arctic Report Card: Update for 2019. doi:10.1007/978-0-387-36699-9_166.

Trefry, J.H., Trocine, R.P., Alkire, M.B., Semmler, C.M., Savoie, M., Rember, R.D., 2009. cANIMIDA Tasks 3 and 4: Sources, concentrations, composition, partitioning and

dispersal pathways for suspended sediments and potential metal contaminants in the coastal Beaufort Sea. Final Report submitted to U.S. Dept. of Interior, Minerals Management Service, Anchorage, Alaska. Contract Nos. M04PC00036 and M04PC0035. 158pp.

Turner, K., Rooper, C.N., Laman, E.A., Rooney, S.C., Cooper, D.W., Zimmermann, M. 2017. Model-based essential fish habitat definitions for Aleutian Island groundfish species. U.S. Dep. Commer., NOAA Tech. Memo. NMFS-AFSC-360, 239 p.

Tweedie, C.E., Aguirre, A., Cody, R., Vargas, S. and Brown, J., 2012, June. Spatial and temporal dynamics of erosion along the Elson Lagoon Coastline near Barrow, Alaska (2002–2011). In Proceedings of the Tenth International Conference on Permafrost, edited by: Hinkel, KM, Salekhard, Yamal-Nenets Autonomous District, Russia (pp. 25-29).

Tweedie, C.E., Escarzaga, S.M., Cody, R.P., Manley, W.F., Gaylord, A.G., Aiken, Q., Lopez, A.F., Aguirre, A., George, C., Nelson, L. and Brown, J., 2016, December. Patterns and Controls of Erosion along the Elson Lagoon Coastline, Barrow, Alaska (2003-2016). In AGU Fall Meeting Abstracts (Vol. 2016, pp. EP12B-02).

U.S. Army Corps of Engineers, Alaska District (USACE) and Environmental Research & Technology, Inc., 1984. Endicott Development Project, Final Environmental Impact Statement Vol II, 781pp.

Vestfals, C.D., Mueter, F.J., Hedstrom, K.S., Laurel, B.J., Petrik, C.M., Duffy-Anderson, J.T. and Danielson, S.L., 2021. Modeling the dispersal of polar cod (*Boreogadus saida*) and saffron cod (*Eleginus gracilis*) early life stages in the Pacific Arctic using a biophysical transport model. Progress in Oceanography, 196, p.102571. https://doi.org/10.1016/j.pocean.2021.102571

Vincent, W.F., Lemay, M. and Allard, M., 2017. Arctic permafrost landscapes in transition: towards an integrated Earth system approach. Arctic Science, 3(2), pp.39-64. https://doi.org/10.1139/as-2016-0027

Wang, T. and Yang, Z., 2020. A Tidal Hydrodynamic Model for Cook Inlet, Alaska, to Support Tidal Energy Resource Characterization. Journal of Marine Science and Engineering, 8(4), p.254.

Weingartner, T.J., Cavalieri, D.J., Aagaard, K. and Sasaki, Y., 1998. Circulation, dense water formation, and outflow on the northeast Chukchi shelf. Journal of Geophysical Research: Oceans, 103(C4), pp.7647-7661.

Weingartner, T.J., Okkonen, S.R., Danielson, S.L. and Region, A.O.C.S., 2009. Circulation and water property variations in the nearshore Alaskan Beaufort Sea. US Department of Interior, Minerals Management Service, Alaska Outer Continental Shelf Region, p. 103.

Weingartner, T.J., Potter, R.A., Stoudt, C.A., Dobbins, E.L., Statscewich, H., Winsor, P. R., Mudge, T.D., Borg, K. 2017. Transport and thermohaline variability in Barrow Canyon on the Northeastern Chukchi Sea Shelf. Journal of Geophysical Research: Oceans, 122, 3565– 3585.

Wolf, S., Reimnitz, E., Barnes, P., 1985. Pleistocene and Holocene Seismic Stratigraphy between the Canning River and Prudhoe Bay, Beaufort Sea, Alaska. Open-File report 85-549. U.S. Geological Survey.

Wong, A.M., Campagnoli, J.G., Cole, M.A., 2007. Assessing 155 years of hydrographic survey data for high resolution bathymetry grids. Pages 1-8 *In* Proceedings of Oceans 2007, Vancouver, B.C., Canada.

Yager, G., 2011. The impact of the Endicott causeway on sediment transport in the Sagavanirktok River Delta, North Slope, Alaska. M.Sc. Thesis., Univ. Alaska Anchorage, 189pp.

Zimmermann, M., Benson, J., 2013. Smooth sheets: How to work with them in a GIS to derive bathymetry, features and substrates. U.S. Dep. Commer., NOAA Tech. Memo. NMFS-249, 52 p.

Zimmermann, M., Reid, J.A., Golden, N., 2016. Using smooth sheets to describe groundfish habitat in Alaskan waters, with specific application to two flatfishes. Deep-Sea Res. II: Understanding Ecosystem processes in the Gulf of Alaska Vol. 1: 210-226.

Zimmermann, M., Prescott, M.M., 2018. Bathymetry and Canyons of the Eastern Bering Sea slope. Geosciences: Special Issue Marine Geomorphometry 8(5), 184. https://doi.org/10.3390/geosciences8050184

Zimmermann, M., Ruggerone, G.T, Freymueller, J.T., Kinsman, N., Ward, D.H., Hogrefe, K., 2018. Volcanic ash deposition, eelgrass beds, and inshore habitat loss from the 1920s to the 1990s at Chignik, Alaska. Estuarine, Coastal and Shelf Science. 202: 69-86. https://doi.org/10.1016/j.ecss.2017.12.001

Zimmermann, M. 2019. Comparison of the physical attributes of the central and eastern Gulf of Alaska IERP inshore study sites. Deep Sea Research Part II: Topical Studies in Oceanography: Understanding Ecosystem Processes in the Gulf of Alaska: Vol. 2. 165:280-291. https://doi.org/10.1016/j.dsr2.2018.05.011

Zimmermann, M., De Robertis, A., Ormseth, O. 2019a. Verification of historical smooth sheet bathymetry. Deep Sea Research Part II: Topical Studies in Oceanography: Understanding Ecosystem Processes in the Gulf of Alaska: Vol. 2. 165:292-302. https://doi.org/10.1016/j.dsr2.2018.06.006

Zimmermann, M., Prescott, M.M, Haeussler, P.J., 2019b. Bathymetry and geomorphology of Shelikof Strait and the western Gulf of Alaska. Geosciences: Special Issue Geological Seafloor Mapping. 9(10), 409. https://doi.org/10.3390/geosciences9100409.

Zimmermann M, Prescott MM. 2021a. False Pass, Alaska: Significant changes in depth and shoreline in the historic time period. Fisheries Oceanography 30:264–279. https://doi.org/10.1111/fog.12517.

Zimmermann M, Prescott MM. 2021b. Passes of the Aleutian Islands: First detailed description. Fisheries Oceanography 30:280–299. https://doi.org/10.1111/fog.12519.

Table 1. Details about historical (1945-53) smooth sheets created from hydrographic surveys. Soundings were collected by fathometers and navigation was conducted by hydrographic sextant (visual triangulation) or Shoran (radio). Horizontal reference systems are discontinued, local datums specific to the Beaufort Sea shore: Barter Island (1948), Flaxman Island (1912), and Barrow (1945). Vertical datum is MLLW (Mean Lower Low Water), which is defined as zero depth. Mean High Water (MHW) shorelines were originally reported in tenths of feet and the unweighted average of all smooth sheets was 0.6 ft (0.17 m). Average MHW values are reported when multiple values were utilized within the area of a smooth sheet. Major corrections to the smooth sheet soundings, such as horizontally shifting them distances in a compass direction due to improper georegistration, or digitizing them, are indicated.

Smooth sheet	Year	Horizontal Datum	Scale	MHW ft/m	Correction
F00109	1952	Barter Island (1948)	1:10,000	0.6/0.18	digitized
H07070	1945	Barter Island (1948)	1:20,000	0.4/0.12	150 m NE
H07071	1945	Barter Island (1948)	1:20,000	0.4/0.12	330 m NE
H07072	1945	Barter Island (1948)	1:20,000	0.4/0.12	330 m NE
H07073	1945	Barter Island (1948)	1:20,000	0.4/0.12	150 m NE
H07074	1945	Barter Island (1948)	1:20,000	0.4/0.12	150 m ENE
H07656	1948	Barter Island (1948)	1:10,000	0.5/0.15	420 m E
H07657	1948, '52	Barter Island (1948)	1:20,000	0.5/0.15	420 m E
H07658	1948, '52	Barter Island (1948)	1:20,000	0.5/0.15	440 m E
H07659	1948	Barter Island (1948)	1:20,000	0.5/0.15	230 m SE
H07756	1949-50	Flaxman Island (1912)	1:20,000	0.7/0.21	325 m SW
H07757	1949-50	Flaxman Island (1912)	1:20,000	0.7/0.21	320 m SW
H07758	1949	Flaxman Island (1912)	1:20,000	0.7/0.21	330 m SW
H07760	1949-50	Flaxman Island (1912)	1:20,000	0.5/0.15	9300 m SW
H07761	1949-50	Flaxman Island (1912)	1:40,000	0.6/0.18	digitized
H07851	1949-50	Flaxman Island (1912)	1:20,000	0.7/0.21	170 m SW

H07852	1950	Flaxman Island (1912)	1:20,000	0.7/0.21	360 m SW
H07853	1950	Flaxman Island (1912)	1:20,000	0.7/0.21	200 m SW
H07854	1950-51	Flaxman Island (1912)	1:20,000	0.5/0.15	1000 m S
H07855	1950	Flaxman Island (1912)	1:40,000	0.7/0.21	200 m SW
H07856	1950-51	Flaxman Island (1912)	1:40,000	0.5/0.15	110 m SW
H07857	1950	Flaxman Island (1912)	1:20,000	0.5/0.15	290 m SW
H07859	1950-51	Barrow (1945)	1:40,000	0.5/0.15	150 m NE
H07915	1951	Flaxman Island (1912)	1:40,000	0.7/0.21	120 m SW
H07916	1951	Flaxman Island (1912)	1:20,000	0.7/0.21	120 m SW
H07917	1951	Flaxman Island (1912)	1:20,000	0.7/0.21	100 m SW
H07918	1951	Flaxman Island (1912)	1:20,000	0.55/0.17	230 m SW
H07919	1951	Barrow (1945)	1:20,000	0.5/0.15	330 m ENE
H07920	1951-52	Barrow (1945)	1:40,000	0.5/0.15	150 m ENE
H07921	1951-52	Barrow (1945)	1:40,000	0.4/0.12	300 m ENE
H07922	1951-53	Barrow (1945)	1:40,000	0.4/0.12	200 m NE
H07979	1952	Barter Island (1948)	1:20,000	0.6/0.18	430 m E
H07980	1952	Barter Island (1948)	1:20,000	0.6/0.18	430 m E
H07981	1952	Barter Island (1948)	1:20,000	0.6/0.18	200 m E
H07982	1952	Barter Island (1948)	1:20,000	0.7/0.21	200 m E
H07983	1952	Barter Island (1948)	1:40,000	0.6/0.18	450 m ESE
H07984	1952	Barter Island (1948)	1:40,000	0.65/0.20	190 m E
H07991	1952	Barrow (1945)	1:40,000	0.55/0.17	180 m E
H08058	1953	Barrow (1945)	1:40,000	0.55/0.17	350 m ENE

H08059	1953	Barrow (1945)	1:80,000	0.7/0.21	200 m NE

Table 2. Details about recent hydrographic surveys.

Survey	Year	Horizontal Datum	Vertical Datum	Scale	Method
D00168	2012	NAD83	MLLW	1:40,000	Multibeam
F00666	2015	NAD83	MLLW	1:20,000	Multibeam
Endicott	1985	Not specified; assumed NAD83	Not specified; assumed MSL	--	Singlebeam
Coastal Frontiers	1997	Alaska State Plane Zone 3, NAD83	MLLW	--	Singlebeam
Arey Lagoon	2011	WGS84	MSL	--	Singlebeam
Elson Lagoon	2015	NAD83(2011) Ellipsoid	GRS80 Ellipsoid	--	Singlebeam
UAF	2018	WGS84(G1762)	MSL	--	Multibeam Thinned to 50 ft× 50 ft Grid Singlebeam
Coastal Frontiers Corporation/BPXA	2013	Alaska State Plane, Zone 3, NAD 83,	MLLW		Singlebeam

Table 3. Summary statistics of depth of closure estimates using ERA5 reanalysis data between 1979 and 2019.

Parameter		Barrow	Foggy Island Bay	Barter Island
inner DOC	mean (m)	3.00 ± 0.70	2.90 ± 0.80	3.20 ± 0.70
	trend* (m/yr)	*0.03*	0.01	0.02
outer DOC	mean (m)	9.25 ± 2.90	6.15 ± 1.85	7.00 ± 1.70
	trend* (m/yr)	*0.15*	*0.06*	*0.06*

*italicized values denote statistically significant trends ($pval \leq 0.05$)

Figure captions

Figure 1. A) Beaufort Sea coast study area, with inset overview map, showing locations of postWorld War II National Ocean Service (NOS) smooth sheets, recent multibeam surveys, and locations of study regions. B) Stefansson Sound region 1985, 1997, and 2018 singlebeam tracklines. C) Barter Island region 2011 singlebeam tracklines. D) Utqiagvik region 2015 singlebeam tracklines.

Figure 2. Depth differences between post-World War II (1945-53) and recent (2012-15) hydrographic surveys in the Utqiagvik region. Warm colors (yellow to red) indicate erosion, whereas cool colors (teal to blue) indicate deposition. Bathymetric contours were generated from post-World War II era NOS smooth sheet bathymetry raster, shoreline change is from Gibbs and Richmond (2017), and the land is from IFSAR (Interferometric Synthetic Aperture Radar: https://elevation.alaska.gov/).

Figure 3A. Depth differences between post-World War II (1945-53) and recent (1997) hydrographic surveys in the Stefansson Sound region. Warm colors (yellow to red) indicate erosion, whereas cool colors (teal to blue) indicate deposition. Bathymetric contours were generated from post-World War II era NOS smooth sheet bathymetry raster, shoreline change is from Gibbs and Richmond (2017), and the land is from IFSAR (Interferometric Synthetic Aperture Radar: https://elevation.alaska.gov/).

Figure 3B. Depth differences between post-World War II hydrographic (1945-53) and a recent (2018) multibeam survey in the Stefansson Sound region. Warm colors (yellow to red) indicate erosion, whereas cool colors (teal to blue) indicate deposition. Bathymetric contours were generated from post-World War II era NOS smooth sheet bathymetry raster, shoreline change is from Gibbs and Richmond (2017), and the land is from IFSAR (Interferometric Synthetic

Aperture Radar: https://elevation.alaska.gov/). Boulder patch rock coverage digitized from Bonsell and Dunton, 2018.

Figure 4. Depth differences between post-World War II (1945-53) and a recent (2011) hydrographic survey in the Barter Island region. Warm colors (yellow to red) indicate erosion, whereas cool colors (teal to blue) indicate deposition. Bathymetric contours were generated from post-World War II era NOS smooth sheet bathymetry raster, shoreline change is from Gibbs and Richmond (2017), and the land is from IFSAR (Interferometric Synthetic Aperture Radar: https://elevation.alaska.gov/).

Figure 5. Scatter plots showing overall depth change in (A) Elson Lagoon, (B) Stefansson Sound, and the (C) Barter Island region. Diagonal lines show the 1:1 fit (dashed) and least-squares linear fit (solid) between the two datasets (linear fit on the UAF 2018 is shown in (B)). The horizontal dashed lines in (B) and (C) show the 41-year (1979 to 2019) upper bounds of the inner (h_{in}) and outer (h_{out}) depths of closure (Table 3 Section 4.2) as they relate to the modern bathymetry. h_{in} represents the approximate seaward limit where nearshore waves and wave-induced currents are expected to dominate sediment transport; h_{out} marks the transition where the influence of wave action on cross-shore sediment transport is likely to be insignificant.

Figure 6. Overview of sediment mobility due to currents and bottom shear stresses. A) Maximum near-bed currents as computed with a three-dimensional numerical model (Curchitser et al., 2017; see text for further details) during September 1998. B-D) Seabed sediment grain sizes and contours of maximum bottom shear stresses computed with the same model as in A) in the vicinity of Utqiagvik, Stefansson Sound, and Barter Island (grain size sources: USGS and usSEABED; Buczkowski et al., 2020a; 2020b). Sediment samples symbolized with circles are subject to resuspension and transport by the modeled currents in A, when compared to threshold

for sediment motion (E). E) Non-cohesive sediment grain sizes plotted against bottom shear stresses modeled with the ROMS model for the three study regions. The black solid lines show the upper and lower limit thresholds of motion for all combinations of varying salinities (25psu to 35psu) and temperatures (2°C to 10°C).

Figure 7. Depth-of-closure estimates computed over the time period 1979 to 2019 using hourly ERA5 reanalysis wave conditions offshore of Utqiagvik, Stefansson Sound, and Barter Island.

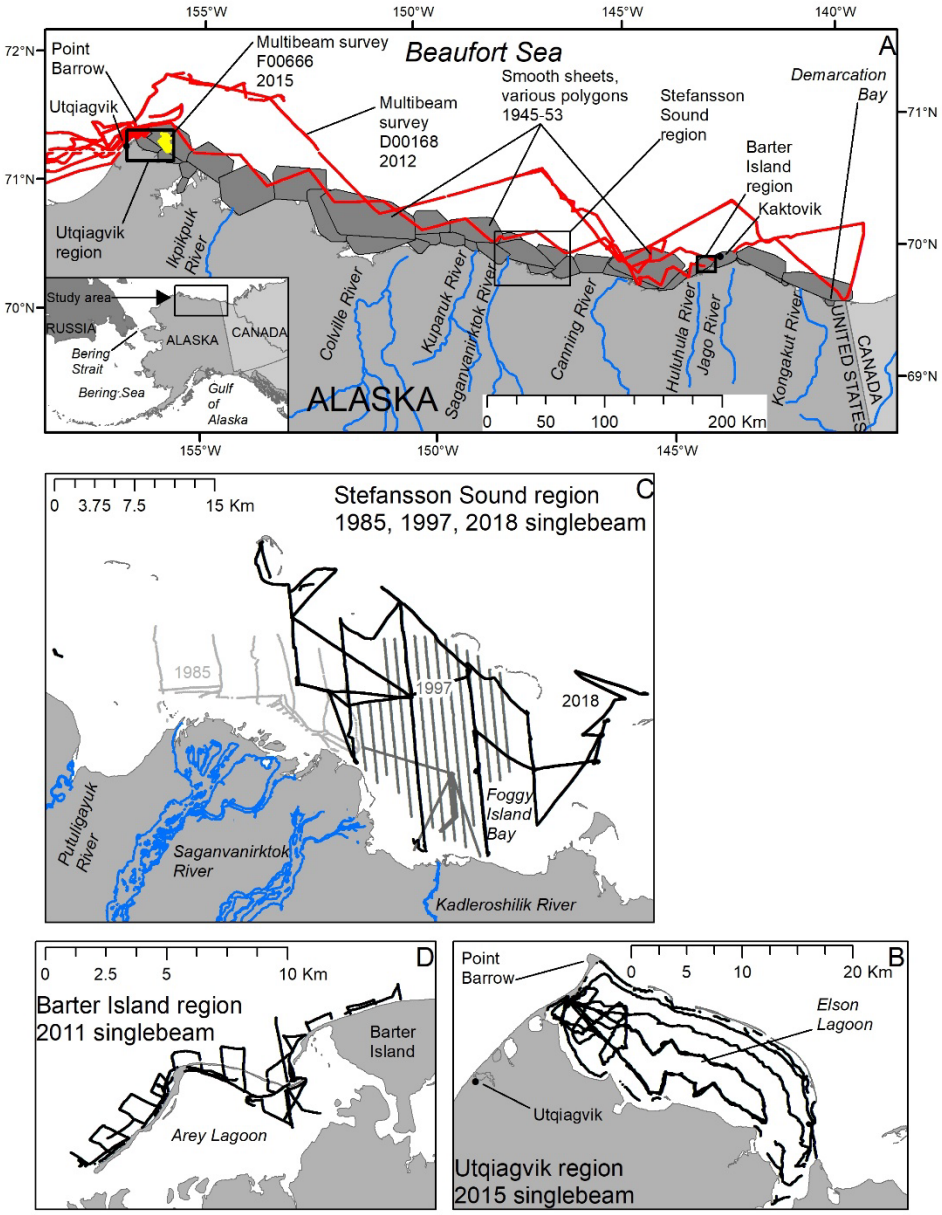

Figure 1. A) Beaufort Sea coast study area, with inset overview map, showing locations of post-World War II National Ocean Service (NOS) smooth sheets, recent multibeam surveys, and locations of study regions. B) Utqiagvik region 2015 singlebeam tracklines. C) Stefansson Sound

region 1985, 1997, and 2018 singlebeam tracklines. D) Barter Island region 2011 singlebeam tracklines.

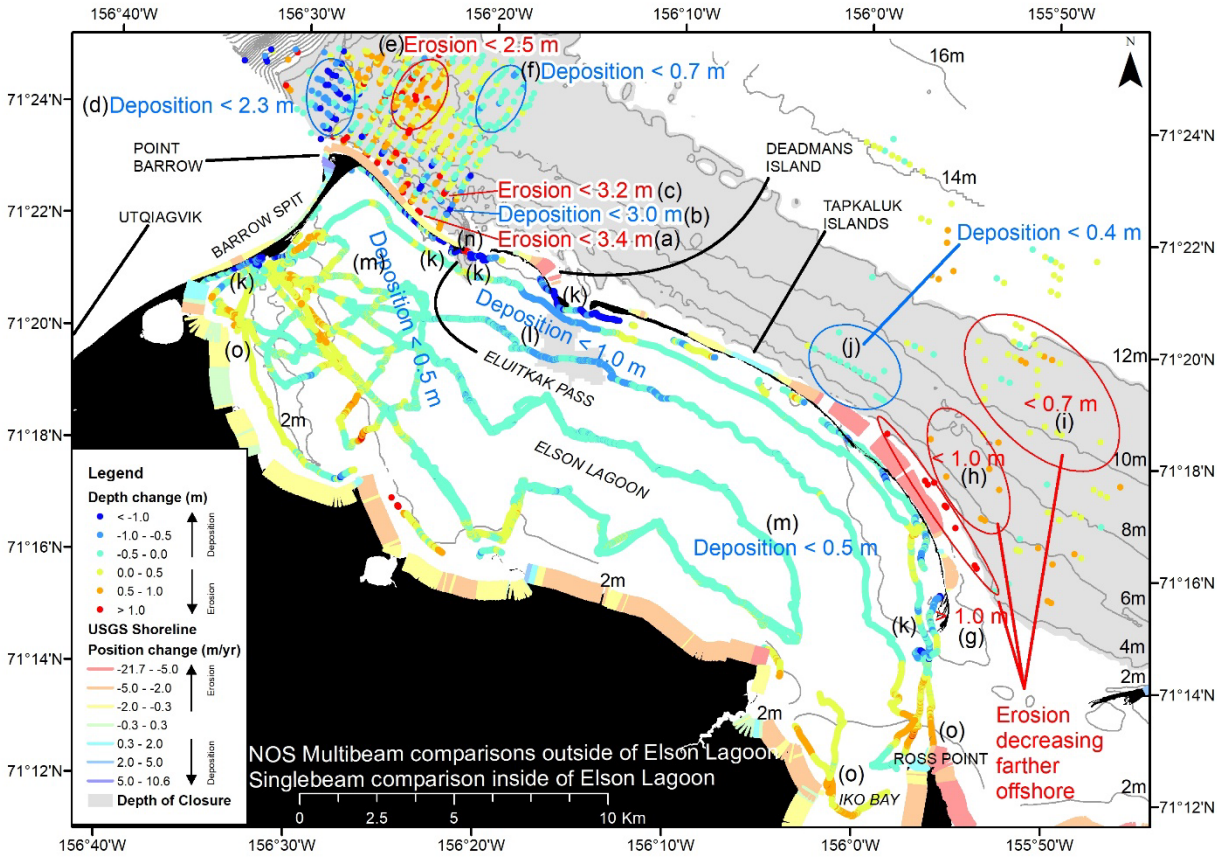

Figure 2. Depth differences between post-World War II (1945-53) and recent (2012-15) hydrographic surveys in the Utqiagvik region. Warm colors (yellow to red) indicate erosion, whereas cool colors (teal to blue) indicate deposition. Bathymetric contours were generated from post-World War II era NOS smooth sheet bathymetry raster, shoreline change is from Gibbs and Richmond (2017), and the land is from IFSAR (Interferometric Synthetic Aperture Radar: https://elevation.alaska.gov/).

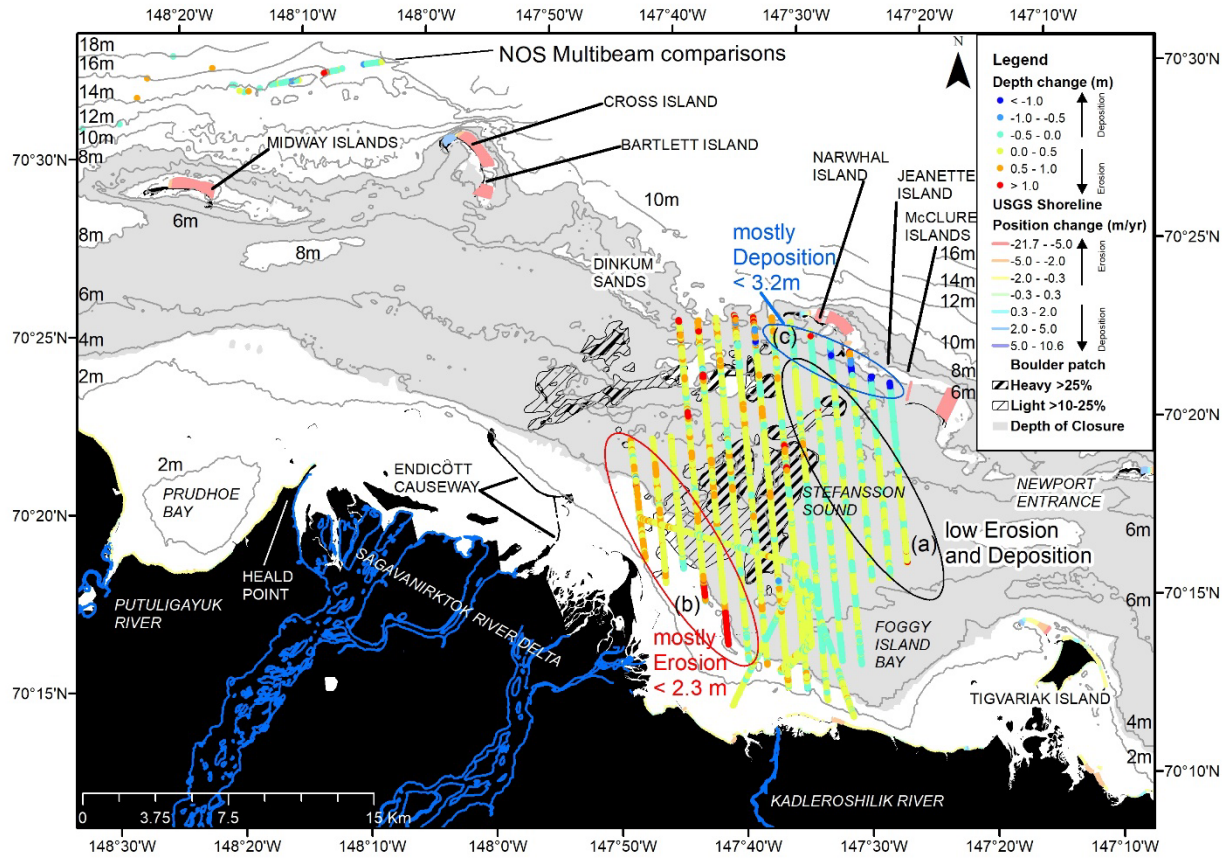

Figure 3A. Depth differences between post-World War II (1945-53) and recent (1997) hydrographic surveys in the Stefansson Sound region. Warm colors (yellow to red) indicate erosion, whereas cool colors (teal to blue) indicate deposition. Bathymetric contours were generated from post-World War II era NOS smooth sheet bathymetry raster, shoreline change is from Gibbs and Richmond (2017), and the land is from IFSAR (Interferometric Synthetic Aperture Radar: https://elevation.alaska.gov/).

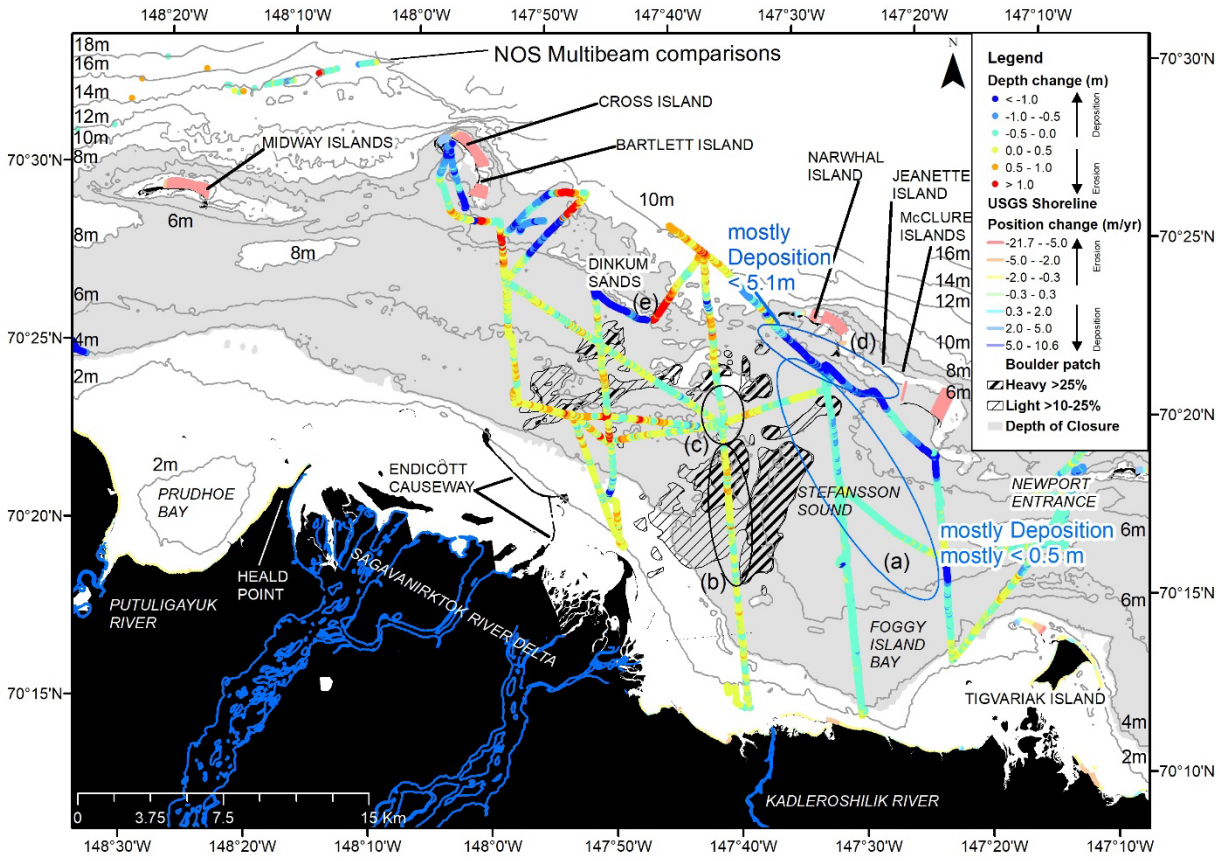

Figure 3B. Depth differences between post-World War II hydrographic (1945-53) and a recent (2018) multibeam survey in the Stefansson Sound region. Warm colors (yellow to red) indicate erosion, whereas cool colors (teal to blue) indicate deposition. Bathymetric contours were generated from post-World War II era NOS smooth sheet bathymetry raster, shoreline change is from Gibbs and Richmond (2017), and the land is from IFSAR (Interferometric Synthetic Aperture Radar: https://elevation.alaska.gov/). Boulder patch rock coverage digitized from Bonsell and Dunton, 2018.

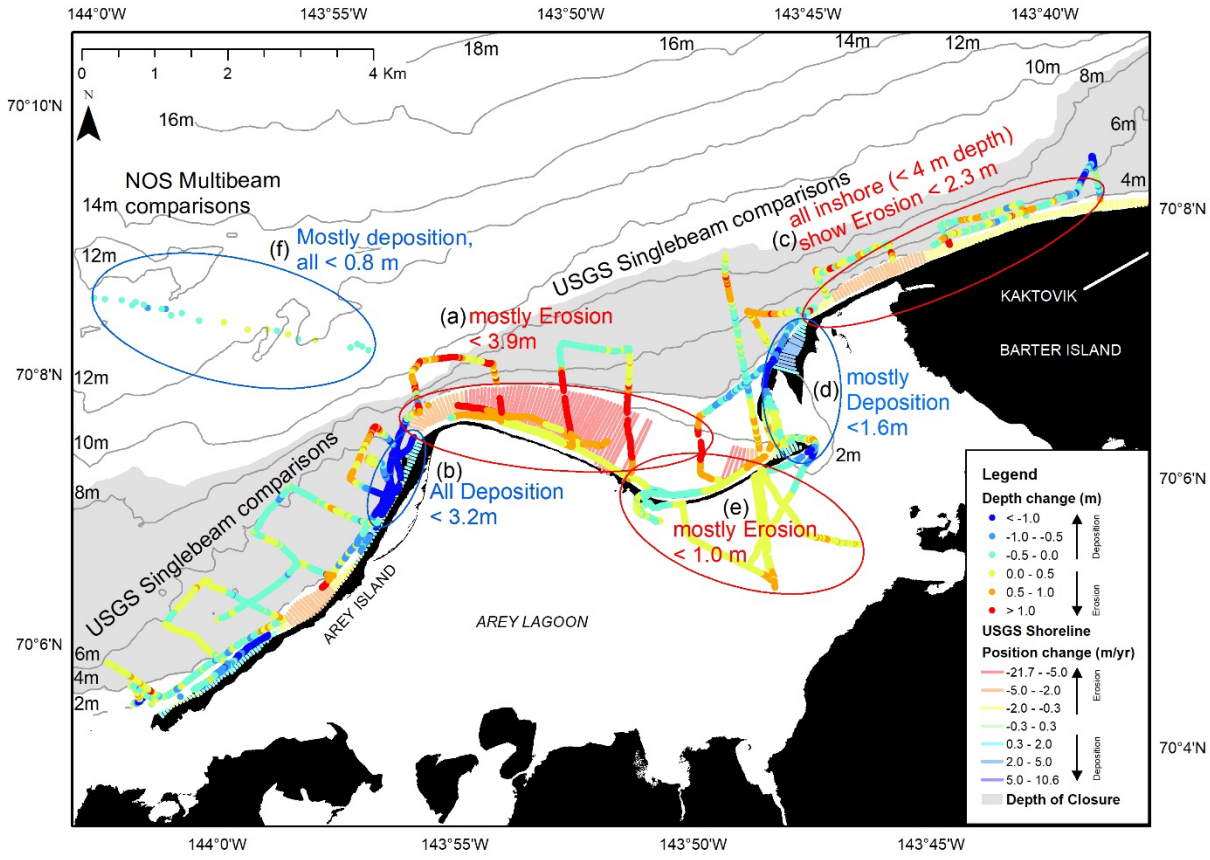

Figure 4. Depth differences between post-World War II (1945-53) and a recent (2011) hydrographic survey in the Barter Island region. Warm colors (yellow to red) indicate erosion, whereas cool colors (teal to blue) indicate deposition. Bathymetric contours were generated from post-World War II era NOS smooth sheet bathymetry raster, shoreline change is from Gibbs and Richmond (2017), and the land is from IFSAR (Interferometric Synthetic Aperture Radar: https://elevation.alaska.gov/).

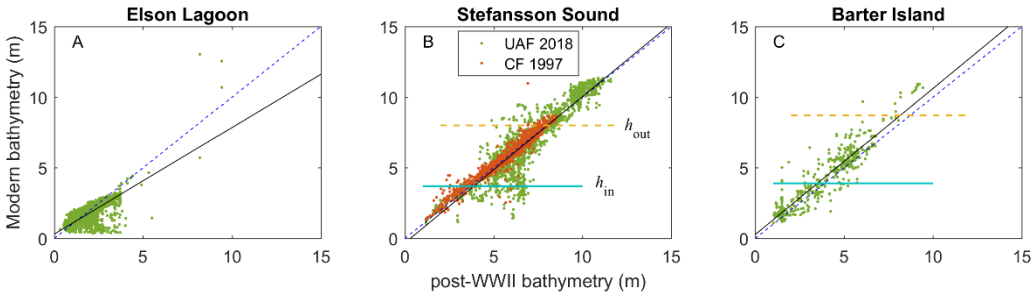

Figure 5. Scatter plots showing overall depth change in (A) Elson Lagoon, (B) Stefansson Sound, and the (C) Barter Island region. Diagonal lines show the 1:1 fit (dashed) and least-squares linear fit (solid) between the two datasets (linear fit on the UAF 2018 is shown in (B)). The horizontal dashed lines in (B) and (C) show the 41-year (1979 to 2019) upper bounds of the inner (h_{in}) and outer (h_{out}) depths of closure (Table 3 Section 4.2) as they relate to the modern bathymetry. h_{in} represents the approximate seaward limit where nearshore waves and wave-induced currents are expected to dominate sediment transport; h_{out} marks the transition where the influence of wave action on cross-shore sediment transport is likely to be insignificant.

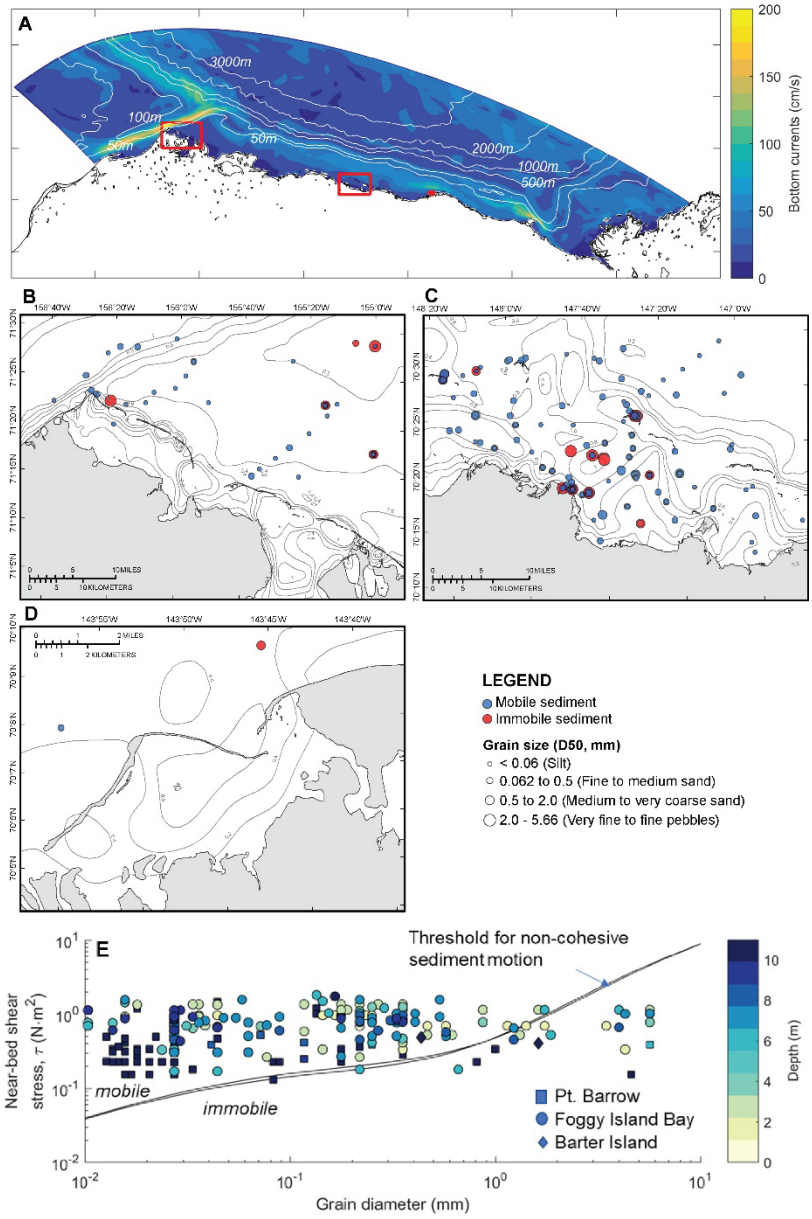

Figure 6. Overview of sediment mobility due to currents and bottom shear stresses. A) Maximum near-bed currents as computed with a three-dimensional numerical model (Curchitser et al., 2017; see text for further details) during September 1998. B-D) Seabed sediment grain sizes and contours of maximum bottom shear stresses computed with the same model as in A) in the vicinity of Utqiagvik, Stefansson Sound, and Barter Island (grain size sources: USGS and usSEABED; Buczkowski et al., 2020a; 2020b). Sediment samples symbolized with circles are subject to resuspension and transport by the modeled currents in A, when compared to threshold for sediment motion (E). E) Non-cohesive sediment grain sizes plotted against bottom shear stresses modeled with the ROMS model for the three study regions. The black solid lines show the upper and lower limit thresholds of motion for all combinations of varying salinities (25psu to 35psu) and temperatures (2°C to 10°C).

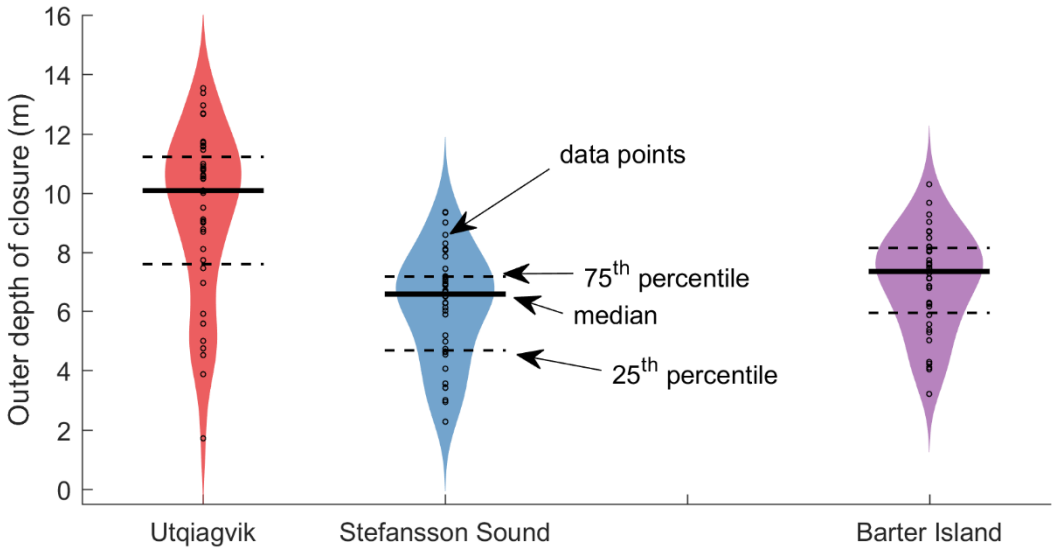

Figure 7. Depth-of-closure estimates computed over the time period 1979 to 2019 using hourly ERA5 reanalysis wave conditions offshore of Utqiagvik, Stefansson Sound, and Barter Island.